

國立交通大學

應用化學系

博士論文

核 / 殼結構量子點之光物理特性與應用

The Photophysical Properties and Applications of Core/Shell Quantum
Dots



研究生：周宜萱

指導教授：裘性天 博士

指導教授：周必泰 博士

指導教授：莊琇惠 博士

中華民國九十四年七月

核 / 殼 結 構 量 子 點 之 光 物 理 特 性 與 應 用
The Photophysical Properties and Applications of Core/Shell Quantum
Dots

研 究 生：周宜萱

Student : Yi-Hsuan Chou

指 導 教 授：裘性天 博士

Advisor : Dr. Hsin-Tien Chiu

指 導 教 授：周必泰 博士

Advisor : Dr. Pi-Tai Chou

指 導 教 授：莊琇惠 博士

Advisor : Dr. Shiow-Huey Chuang

國 立 交 通 大 學
應 用 化 學 系
博 士 論 文



Submitted to Department of Applied Chemistry
College of Science

National Chiao Tung University

in partial Fulfillment of the Requirements

for the Degree of

Academic

in

Applied Chemistry

July 2005

Hsinchu, Taiwan, Republic of China

中 華 民 國 九 十 四 年 七 月

授權書

(博碩士論文)

本授權書所授權之論文為本人在 國立交通大學 應用化學 所

無機化學 組 九十四 學年度第 二 學期取得 博 士學位之論文。

論文名稱：核/殼結構量子點之光物理特性與應用
The Photophysical Properties and Applications of Core/Shell Quantum Dots

1. 同意 不同意

本人具有著作財產權之論文全文資料，授予行政院國家科學委員會科學技術資料中心、國家圖書館及本人畢業學校圖書館，得不限地域、時間與次數以微縮、光碟或數位化等各種方式重製後散布發行或上載網路。

本論文為本人向經濟部智慧財產局申請專利的附件之一，請將全文資料延後兩年後再公開。(請註明文號：)

2. 同意 不同意

本人具有著作財產權之論文全文資料，授予教育部指定送繳之圖書館及本人畢業學校圖書館，為學術研究之目的以各種方法重製，或為上述目的再授權他人以各種方法重製，不限地域與時間，惟每人以一份為限。

上述授權內容均無須訂立讓與及授權契約書。依本授權之發行權為非專屬性發行權利。依本授權所為之收錄、重製、發行及學術研發利用均為無償。上述同意與不同意之欄位若未鈎選，本人同意視同授權。

指導教授姓名： 裘性天 博士
周必泰 博士
莊琇惠 博士

研究生簽名： 學號：8925802
(親筆正楷) (務必填寫)

日期：民國 94 年 7 月 日

1. 本授權書請以黑筆撰寫並影印裝訂於書名頁之次頁。
2. 授權第一項者，所繳的論文本將由註冊組彙總寄交國科會科學技術資料中心。
3. 本授權書已於民國 85 年 4 月 10 日送請內政部著作權委員會（現為經濟部智慧財產局）修正定稿。
4. 本案依據教育部國家圖書館 85.4.19 台(85)圖編字第 712 號函辦理。

核 / 殼 結 構 量 子 點 之 光 物 理 特 性 與 應 用

學生：周宜萱

指導教授：裘性天 博士

周必泰 博士

莊琇惠 博士

國立交通大學應用化學所 博士班

摘 要

在本論文中我們研究一系列的二-六族半導體核/殼量子點材料。其中包含了第一型和第二型的殼/核量子點之合成方法、材料特性以及應用的探討。

透過便利、且單鍋合成的方法，我們以氧化鎘(CdO)為前驅物合成出第一型的 CdSe@ZnX (X = S, Se) 的核/殼量子點。為了拓展應用性，我們進一步製備出水溶性的量子點並分別應用於固/液相之金屬離子檢測系統以及分子間能量傳遞系統等兩方面。以上所述之各種核/殼量子點材料、系統之物理、化學特性亦有詳細的探討。

第二型的 CdSe@ZnTe 和 CdTe@CdSe 核/殼量子點，是以較為環保的氧化鎘(CdO)與氯化鎘(CdCl₂)分別為製備核/殼的前驅物來合成。在此，對於層間放光的光譜與動力學解析我們有進一步的研究。此外，利用飛秒雷射的增益轉換技術，我們首度觀察到 CdTe@CdSe 層間放光的初期緩解動力學現象；此現象指出，第二型的核/殼量子點其電子電洞分離速率會與核心大小呈反比。我們可將此結果應用於電子電洞分離速率的控制並應用於光電元件的材料設計上。我們亦研究同屬第二型的三層核/殼量子點 CdSe@ZnTe@ZnS and CdSe@CdTe@ZnTe 的合成與其物、化特性。CdSe@ZnTe@ZnS 建基於 CdSe@ZnTe 的雙層結構之上；藉由硫化鋅(ZnS)的包覆，雖然造成 CdSe@ZnTe 放光波長的小小紅移現象，卻大大地提高其量子產率到原來的 30 倍強。如此一來，我們成功製備出屬於第二型的層間放光特性，卻具有接近第一型量子產率的核/殼/殼量子點，開拓了相同核/殼量子點材料之波長調控度。另一方面，我們在 CdSe@ZnTe 的雙層結構之間插入另一層 CdTe 層，此舉乃是為了讓電子電洞分離更形徹底；藉由 CdTe 夾心層的存在，使得電子電洞的結合更為不易。在 CdSe@ZnTe 的雙層結構時，電子電洞結合的輻射生命期由單一 CdSe 的奈米秒級延長至微微秒級；而在三層結構 CdSe@CdTe@ZnTe 中，更大幅延長至 10 個毫秒左右。我們相信這個改良對於光電元件的光電轉換效能應有顯著之影響。

The Photophysical Properties and Applications of Core/Shell Quantum Dots

Student : Yi-Hsuan

Advisors : Dr. Hsin-Tien Chiu

Dr. Pi-Tai Chou

Dr. Shiow-Huey Chuang

Department of Applied Chemistry
National Chiao Tung University

ABSTRACT

In this thesis we report the syntheses, characterizations and applications of various II-VI semiconductor core/shell Quantum dots (QDs), including type I and type II QDs.

The synthesis of CdSe@ZnX (X=S,Se) core/shell QDs from the CdO precursor through a convenient, one-pot approach. For the view point of applications, we have demonstrated two practical systems one is based on DHLA capped CdSe@ZnS (core/shell) QDs to fluorogenically probe Hg²⁺ in aqueous solution and solid film at room temperature. Submicromolar sensitivity has been achieved promptly with this system. The other approach is to modify the CdSe@ZnS QDs with 15-crown-5 in water exhibit excellent selectivity toward K⁺.

Type II CdSe@ZnTe and CdTe@CdSe QDs are prepared from the greener CdO and CdCl₂ precursors for core and shell, respectively. The spectroscopy and dynamics of these type-II QDs interband emissions are studied. The hole transfer rate of CdSe@ZnTe as a function of the core/shell size has been systematically investigated. Based on the femtosecond upconversion technique, the first early relaxation dynamics on the CdTe/CdSe type-II QDs interband emission is observed. The results indicate that the electron separation rate decreases as the size of the cores increases. We believed that the degree of control on the rate of electron transfer can be crucial in applications where rapid carrier separation followed by charge transfer into a matrix or electrode is important, as in photovoltaic devices.

In addition, syntheses of CdSe@ZnTe@ZnS and CdSe@CdTe@ZnTe (core/shell/shell) type-II QDs from CdSe@ZnTe and CdSe@CdTe, respectively, have been achieved. In comparison to that

of type-II CdSe@ZnTe, although the addition of ZnS only changed the interband emission peak wavelength slightly, due to the quantum confinement for CdSe \rightarrow ZnTe interband emission, type-II CdSe@ZnTe@ZnS gives rise to \sim 30 folds enhancement of the quantum efficiency. Next, comparing with the strong CdSe emission, moderate CdSe \rightarrow CdTe emission for CdSe@CdTe, rather weak CdSe \rightarrow ZnTe interband emission was resolved for the CdSe@CdTe@ZnTe structure. Capping ZnTe to CdSe@CdTe results in a far electron-hole separation between CdSe and ZnTe via an intermediate layer, CdTe. In the case of CdSe@CdTe@ZnTe structure, a lifetime of as long as 150 ns was observed for the CdSe \rightarrow ZnTe 1415 nm emission. The result further deduces an enormously long radiative lifetime of \sim 10 ms due to the spatial separation of electron and hole via the CdTe intermediate layer. In the case of CdSe@CdTe@ZnTe structure, upon excitation, the float of long-lived charge separation may serve as an excellent hole-carrier for catalyzing the oxidation reaction. Attempts have also been made in synthesizing the ZnTe@CdTe@CdSe type-II QDs, in which the order of band edges is reversed with respect to the CdSe@CdTe@ZnTe structure, so that the electron can be floated in the CdSe layer to carry out the reduction reaction. However, at this stage, this pathway failed due to the difficulty in synthesizing ZnTe core QDs. Focus on circumventing this obstacle is currently in progress.



Table of Content

中文摘要	iv
Abstract	v
Table of Content	vii
Index of Figures	ix
Index of Schemes	xii
Index of Tables	xii
誌謝	xiii
Chapter 1	Introduction of Quantum Dots	1
1.1	Theoretical considerations of bulk and nanocrystal semiconductors.....	3
1.1.1	Bulk semiconductors.....	4
1.1.2	Nanocrystalline semiconductors.....	5
1.2	Reviews of the Applications to Semiconductor QDs.....	8
1.2.1	Applications of Devices.....	8
1.2.2	Optical Properties of Nano-Semiconductor.....	9
1.2.3	Semiconductor QDs as Biological Imaging Agents.....	12
1.2.4	Exceptional surface modification of quantum dots.....	23
1.3	The Backgrounds of Core/Shell Quantum Dots.....	28
1.3.1	Type-I CdSe@ZnS(ZnSe) Core/Shell Quantum Dots.....	28
1.3.1.1	Surface Passivation.....	28
1.3.1.2	Protective Types Core/Shell Structure.....	30
1.3.2	Type-II Core/Shell Quantum Dots.....	32
1.3.3	Type-II Core/Shell/Shell Quantum Dots.....	34
1.4	The Applications of Core/Shell QDs Efforted in This Thesis.....	36
1.4.1	The Metal Ion Probes.....	36
1.4.2	Intermolecular Energy Transfer System.....	38
1.5	References.....	42
Chapter 2	Type-I CdSe@ZnX (X=S, Se) Core/Shell Quantum Dots and their Applications	50
2.1	Introduction.....	50
2.2	Experimental Section.....	53
2.2.1	Chemicals.....	53
2.2.2	Method 1 - Size Tuning.....	53
2.2.3	Method 2 – Size Uniform.....	55
2.2.4	Water-Soluble Synthetic Procedure.....	56
2.2.4.1	DHLA Capping.....	56
2.2.4.2	Crown-Dithiolcapping.....	57
2.2.5	Measurement.....	58
2.3	Results and Discussion.....	59
2.3.1	Reaction Parameters.....	59
2.3.2	Products Characterization.....	63
2.3.3	Comparing Current Methods.....	67

2.3.4	Preparation and Application of DHLA capped CdSe@ZnS QDs.....	69
2.3.5	Preparation and Application of 15-Crown-5 Functionalized CdSe@ZnS Quantum Dots.....	74
2.4	Conclusions.....	80
2.5	References.....	82
2.6	Appendix.....	88
Chapter 3	Type-II CdSe@ZnTe and CdTe@CdSe Core/Shell Quantum Dots and their Properties.....	90
3.1	Introduction.....	90
3.2	Experimental Section.....	90
3.2.1	Chemicals.....	90
3.2.2	Synthetic procedure.....	91
3.2.2.1	CdSe@ZnTe QDs.....	91
3.2.2.2	CdTe@CdSe QDs.....	92
3.2.3	Measurement.....	93
3.3	Results and Discussion.....	95
3.3.1	CdSe@ZnTe QDs.....	95
3.3.2	CdTe@CdSe QDs.....	101
3.4	Conclusions.....	110
3.5	References.....	112
Chapter 4	Syntheses and Photophysical Properties of Type-II CdSe@ZnTe@ZnS and CdSe@CdTe@ZnTe Core/Shell/Shell Quantum Dots.....	113
4.1	Introduction.....	113
4.2	Experimental Section.....	114
4.2.1	Chemicals.....	114
4.2.2	Synthetic procedure.....	114
4.2.2.1	CdSe@ZnTe@ZnS QDs.....	114
4.2.2.2	CdSe@CdTe@ZnTe QDs.....	115
4.2.3	Measurement.....	117
4.3	Results and Discussion.....	118
4.3.1	CdSe@ZnTe@ZnS QDs.....	118
4.3.2	CdSe@CdTe@ZnTe QDs.....	125
4.4	Conclusions.....	133
4.5	References.....	134
Chapter 5	Concluding Remarks.....	136
5.1	Studies Related to Type-I CdSe@ZnX (X=S, Se) Core/Shell QDs.....	136
5.2	Studies Related to Type-II CdSe@ZnTe and CdTe@CdSe Core/Shell QDs...	137
5.3	Studies Related to Type-II CdSe@ZnTe@ZnS and CdSe@CdTe@ZnTe Core/Shell/Shell QDs.....	138

Index of Figures

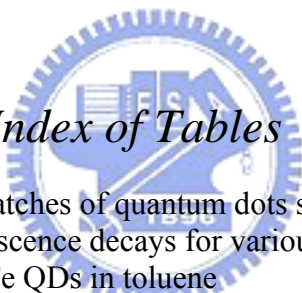
Figure 1.1	Size relationships of atoms, nanoparticles, and condensed matter	1
Figure 1.2	Schematic illustration of the density of states in metal and semiconductor clusters.	2
Figure 1.3	Idealized density of states for one band of a semiconductor structure of 3, 2, 1, and “0” dimensions.	3
Figure 1.4	Electroluminescence from single monolayers of nanocrystals in molecular organic devices.	8
Figure 1.5	Hybrid Nanorod-Polymer Solar Cells	8
Figure 1.6	(a) Chemical structure of OC ₁ C ₁₀ -PPV. (b) Photovoltaic device structure.	9
Figure 1.7	Schematics of “absorbing” and “emitting” transitions in CdSe QDs along with intraband relaxation processes leading to a population buildup of the “emitting” transition.	9
Figure 1.8	Excitation across the band gap by photon absorption: (a) direct process; (b) indirect process.	12
Figure 1.9	Size- and materials-dependent emission spectra of several surfactant-coated semiconductor nanocrystals in a variety of sizes.	13
Figure 1.10	Mouse 3T3 Fibro-plast labeled with color- tunable QDs.	14
Figure 1.11	ZnS-capped CdSe QDs that is covalently coupled to a protein by mercaptoacetic acid.	14
Figure 1.12	The generation of DNA-linked QDs assemblies.	15
Figure 1.13	Schematic of the FRET binding assay mechanism and normalized absorption and emission spectra.	16
Figure 1.14	Uptake and transport of QDs by breast tumor cells using confocal microscopy.	16
Figure 1.15	(Up) the distinguishable emission colors of CdSe@ZnS QDs excited with a near-UV lamp; (down) schematic illustration of bioconjugation methods.	17
Figure 1.16	Design of QDs coated with either peptides only or with peptides and PEG, then intravenous delivery of this QDs into specific tissues of the mouse.	18
Figure 1.17	Schematic of single-QDs encapsulation in a phospholipids block-copolymer micelle and QDs-micelle conjugation with single-stranded DNA (ssDNA).	18
Figure 1.18	Deep tissue imaging of a vasculature system.	20
Figure 1.19	Three strategies for bioconjugation to QDs probe.	21
Figure 1.20	Microbead containing various levels of CdSe@ZnS QDs.	22
Figure 1.21	Recombinant protein linker contains a functional protein moiety, MBP, and a basic leucine zipper motif.	22
Figure 1.22	Formation of the polymer-QDs showing and idealized micellar polymer shell (40% octylamine- modified PAA) encapsulating the QDs.	24
Figure 1.23	Schematic illustration of bioconjugated QDs for on vivo cancer targeting by modified polymer on surface.	24
Figure 1.24	QDs surfaces modification and modifying the surface charge arbitrarily by coating different polymer.	25
Figure 1.25	Four key compounds used of Peng’s work.	26
Figure 1.26	One-pot formation of amine box nanocrystals.	27
Figure 1.27	Schematic procedure for the formation of avidin-biotin/box nanocrystal conjugates.	27
Figure 1.28	Nanocrystal surrounded by TOPO chains anchored to its surface.	28
Figure 1.29	Common emission mechanism of the semiconductor nanocrystal.	29
Figure 1.30	Bared CdSe QDs and inorganic surface passivation core/shell type-I QDs.	30
Figure 1.31	Comparison of stability of core and two types of core/shell QDs.	31
Figure 1.32	Summary of the band offsets (in eV) and lattice mismatch (in %) between the	31

	InAs core and other shells.	
Figure 1.33	Illustrations of the energy band gap difference between (A) type-I and (B) type-II QDs.	33
Figure 1.34	Metal ion probe by the organic fluorophore anchored with aza-crown.	38
Figure 1.35	Heavy-metal ion recognition and binding of the functionalized gold nanoparticle.	38
Figure 1.36	Colorimetric responses for metal ion recognition.	38
Figure 1.37	Structural formula of FHP6 and the reference compound FHP1.	39
Figure 1.38	Concentration-dependent fluorescence spectra of an equal molar mixture of two compounds in CHCl ₃ .	40
Figure 1.39	Fluorescence Resonance Energy Transfer Analysis of Apolipoprotein E C-Terminal.	41
Figure 2.1	The absorption and emission spectra of DHLA capped CdSe@ZnS (core, 4.1 nm, shell, 1.2 nm) in H ₂ O (pH = 7~8).	57
Figure 2.2	Absorption and emission spectra of CdSe@ZnS in toluene.	59
Figure 2.3	Temporal evolution of the absorption spectrum of the CdS QDs grown in ODE and different OA concentration.	61
Figure 2.4	TEM micrograph of CdSe@ZnS nanocrystals prepared by the tunable-size method.	61
Figure 2.5	EDX and XPS characterization of CdSe@ZnS core/shell nanoparticles.	63
Figure 2.6	Series XRD patterns of core CdSe, and core/shell CdSe@ZnS nanoparticles.	65
Figure 2.7	Synthesis of CdSe/CdS QDs by pyridine coated on the CdSe core.	65
Figure 2.8	Control experiments performed on method 1 (tunable-size) with 6 different aging times (12 aliquots) are compared.	66
Figure 2.9	Emission spectra of two different size 2-(12-Mercaptododecyloxy) methyl-15-crown ether capped CdSe@ZnS nanoparticles in aqueous solution.	67
Figure 2.10	TEM image of core CdSe nanoparticles prepared from the CdO@HDA reaction system.	68
Figure 2.11	The TEM image of DHLA capped CdSe@ZnS nanoparticles before and after adding Hg ²⁺ (1.6 × 10 ⁴ M).	69
Figure 2.12	The fluorescence spectrum of CdSe@ZnS QDs in water (pH ~ 7) by adding Hg(ClO ₄) ₂ .	70
Figure 2.13	The plot of QDs fluorescence as a function of concentrations for various metal-ion salts and anions.	70
Figure 2.14	The tentatively proposed Hg ²⁺ recognition mechanisms based on DHLA capped CdSe@ZnS QDs.	71
Figure 2.15	The decay dynamics of the QDs in H ₂ O at various added Hg ²⁺ concentrations shown in the insert.	72
Figure 2.16	The decay dynamics of the QDs in H ₂ O at various added Hg ²⁺ concentrations shown in the insert.	75
Figure 2.17	The fluorescence titration spectra of CdSe@ZnS in water by adding Hg(ClO ₄) ₂	76
Figure 2.18	Photographs of (A) 54.9 nM CdSe@ZnS QDs in CH ₃ CN, and (B) subsequently addition of KClO ₄ of 10 ⁻² M. (C) Similar to (B) except for a span of 5 minutes.	77
Figure 2.19	TEM micrographs of 15-crown-5 functionalized CdSe@ZnS QDs (A) before and (B) after addition of 0.1 mM K ⁺ .	77
Figure 2.20	(black) The emission trace of green QDs in a mixture of green and red QDs in H ₂ O. (gray) Similar condition, except for the addition of KClO ₄ .	80
Figure 3.1	TEM images of the CdSe QDs and CdSe@ZnTe QDs.	95
Figure 3.2	Absorption spectra of CdSe core and corresponding CdSe@ZnTe core/shell QDs in toluene.	95
Figure 3.3	Emission spectra of CdSe core QDs and corresponding CdSe@ZnTe core/shell	96

	QDs in toluene.	
Figure 3.4	The fluorescence upconversion signal for CdSe@ZnTe QDs in toluene. Emission is monitored at the peak wavelength of the corresponding core. Insert: The plot of electron-hole interfacial separation rate as a function of the core diameter.	98
Figure 3.5	The steady-state emission of CdSe@ZnTe core/shell QDs (3.5/0.8 nm) excited at 375 nm.	99
Figure 3.6	The same size of CdSe core coated with different thickness of the ZnTe shell. λ_{ex} : 375 nm.	99
Figure 3.7	TEM images of the samples CdTe QDs and CdTe@CdSe QDs.	101
Figure 3.8	EDX and XRD characterization of CdTe core and CdTe@CdSe core/shell nanocrystals prepared from CdCl ₂ precursor.	102
Figure 3.9	The normalized XPS spectra of CdTe@CdSe acquired at different electron takeoff angle of 90° and 54.7°.	103
Figure 3.10	The absorption and emission spectra of CdTe core and CdTe@CdSe core/shell type-II QDs in toluene with different sizes.	104
Figure 3.11	The fluorescence upconversion signal for CdTe@CdSe QDs in toluene with different sizes.	107
Figure 4.1	TEM images of the samples of CdSe@ZnTe QDs and CdSe@ZnTe@ZnS QDs.	119
Figure 4.2	EDX and XRD characterization of CdSe@ZnTe core/shell and CdSe@ZnTe@ZnS core/shell/shell QDs.	120
Figure 4.3	The normalized absorption and emission spectra of CdSe core, CdSe@ZnTe core/shell and CdSe@ZnTe@ZnS core/shell/shell QDs in toluene.	121
Figure 4.4	The absorption and emission spectra of a. TOPO capped CdSe@ZnTe@ZnS QDs in toluene, b. DHLA capped CdSe@ZnTe@ZnS QDs in water (pH ~ 7) and the emission of DHLA capped CdSe@ZnTe@ZnS QDs in water excited by 1200 nm laser pulse.	124
Figure 4.5	The plot of 930-nm peak intensity (I) for DHLA capped CdSe@ZnTe@ZnS as a function of square of excitation power.	124
Figure 4.6	TEM images of the samples of CdSe@CdTe and CdSe@CdTe@ZnTe QDs.	126
Figure 4.7	EDX and XRD characterization of CdSe@CdTe core/shell and CdSe@CdTe@ZnTe core/shell/shell (right) QDs.	127
Figure 4.8	The normalized absorption and emission spectra of CdSe core, CdSe@CdTe core/shell and CdSe@CdTe@ZnTe core/shell/shell QDs in toluene.	129
Figure 4.9	The decay profile of CdSe@CdTe@ZnTe (3.4/1.8/1.3 nm) core/shell/shell QDs in toluene monitored at 1400 ± 20 nm ($\lambda_{\text{ex}} = 532$ nm).	131

Index of Schemes

Scheme 1.1	Plot illustrating the CdTe, CdSe and TiO ₂ band offsets alignment in energy.	34
Scheme 1.2	Plot illustrating the CdSe, CdTe, ZnTe and ZnS band offsets alignment in energy.	35
Scheme 2.1	The synthetic route of preparing MCE.	58
Scheme 2.2	The proposed K ⁺ recognition scheme through an intermolecular MCE-CdSe@ZnS K ⁺ MCE-CdSe@ZnS sandwich type of association.	82
Scheme 4.1	Plot illustrating the alignment of CdSe, CdTe, ZnTe and ZnS band offsets.	113
Scheme 5.1	Summary of Explorations.	135



Index of Tables

Table 2.1	Photophysics of various batches of quantum dots synthesized from this study	60
Table 3.1	Room temperature luminescence decays for various sizes of CdSe and corresponding CdSe@ZnTe QDs in toluene	97
Table 3.2	Room-temperature photophysical properties for various sizes of CdTe and corresponding CdTe@CdSe QDs in toluene	106
Table 4.1	Room-temperature photophysical properties for CdSe, CdSe@ZnTe and corresponding CdSe@ZnTe@ZnS QDs	122
Table 4.2	Room-temperature photophysical properties for CdSe, CdSe@CdTe and CdSe@CdTe@ZnTe QDs in toluene.	130

誌 謝

白雲孤鷺飛盡處 最好暮天秋碧 回首五年間事 多番更替 凝眸幾許
墨竹蟬梵微風倚 又是飄零為客 三徑尋歸何年 憑欄遠眺 西風萬里

要把漫漫五年中，不亞於全校師生人數的感謝名單濃縮在短短的幾百字當中，實在是一件頗為艱鉅的工作。除勒要感謝本所 陳登銘教授及清大 李紫原教授對本論文的修改指正之外；首先必須感謝我的化學啟蒙恩師台大 周必泰教授在我碩、博七年的研究生涯中，持續的關懷、解惑、支持、引導；小子何能，得蒙大師亦師亦友之隆情？感謝指導老師 裘性天教授五年來的悉心指導，在老師自由、開放的觸發式循循善誘下，學生得如初生魚苗悠游探索在浩瀚的學術汪洋中；此外，裘師更以朗朗身教對於「才而性緩、智而氣和」作了最佳示範。感謝高大 莊琇惠助理教授對我的細心栽培、詳加指導、呵護照拂、情盛姐妹。此外，還要再次感謝 李紫原教授在生活上的關注與開解；清大 齊正中教授、台大 張哲政教授、NDL 簡昭欣博士、張茂男博士以及本所 李耀坤教授在各自的專業領域中無私指導；另外，本所 陳月枝副教授、楊耀文副教授、王念夏教授以及 鍾文聖教授適時的慷慨解惑學生亦深銘于心。

感謝好友一字、心泰、阿勇、騰芳、亞玄、嘉琳、Backy、Teddy、盧、永昌、阿財、建良、Chetan 等，因著你們的支持與勸勉使我的博班生涯多采多姿並充滿信心；感謝鄭至玉博士與實驗室：老闆、寶哥、如君、裕煦、俊雄、蔣姐等學長姐的關懷與指導，讓我在面對挫折時能有屢敗屢戰的勇氣；感謝靜雯、隆昇、庭毅、宜鋒、治偉、振宇、政君、Baken、盈薰、(夏)志豪、(黃)志豪、小黑、子厚、小昭、曜安、進興、亭凱、高翔、煌凱、宇婕、蕭蕭以及交大應化四號家族等學弟妹的協助與陪伴，以歡笑填充了生活上原本可能的空白。此外，台大 Chou's lab 的俊彥等、Chang's lab 的錫昌等、NDL 的 Chien's group 明瑞等、清大 Lee's lab 的正得等、還有 Chi's lab 的信霖等夥伴們，過去與你們共同努力與付出的日子都是我不可或忘的美好回憶。

感謝德蘭讀經班、聖神堂、大專青年會等在靈修與精神生活上的共融分享；更要感謝我的家人：沒有父母無怨的付出與明智的指引，以及黎黎的苦樂分享，我實在無法獨自走到此處。

感謝 天主，無時無刻照拂我、引導我、並將上文述及甚或闕漏的人間天使們恩賜給我；願 天主祝福這群人間天使以及所有愛你們與你們所愛的人。阿們！

Chapter 1. Introduction

In the last two decades of the 20th century, a new realm conventionally named “nano-scale”, of matter, which lies between chemistry (molecular properties) and solid-state physics (bulk properties) has been booming with an unexpectedly fast pace. Traditionally, chemistry is the study of atoms and molecules, a territory of substances with dimensions generally less than one nanometer, while condensed matter physics deal with solids of essentially an infinite array of bound atoms or molecules of dimensions greater than 100 nm. For long, there exists a significant gap between these regimes, and one can apply Figure 1.1, in a qualitative manner, to illustrate this gap, in which apparently no continuity had been established in between particles of 1 to 100 nm, or about 10 to 10⁶ atoms or molecules per particle.^{1,2} However, from the end of the 20th century through now on, the merge between the “top-down”(physics) and “bottom-up” processes toward the nano-scale territory has become obvious, and the relevant research has attracted much attention in the fields of chemistry, physics, material science and even molecular biology. Nowadays, “nanoscience” is believed to be the most popular terminology worldwide, and its mission may not be fulfilled without an interdisciplinary team work.

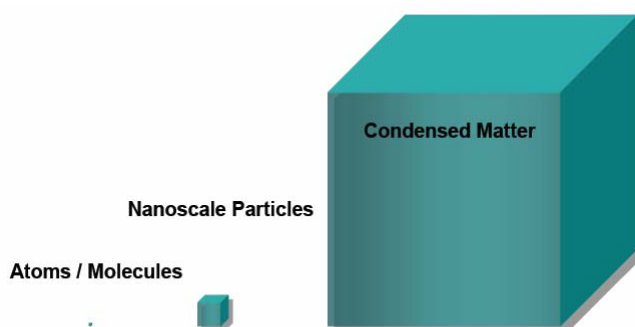


Figure 1.1 Size relationships of atoms, nanoparticles, and condensed matter.

In these nanoscale regimes, particle sizes are between atoms and bulk materials, in which particle was close to molecules level. Two major effects are responsible for these size variations in nanocrystal

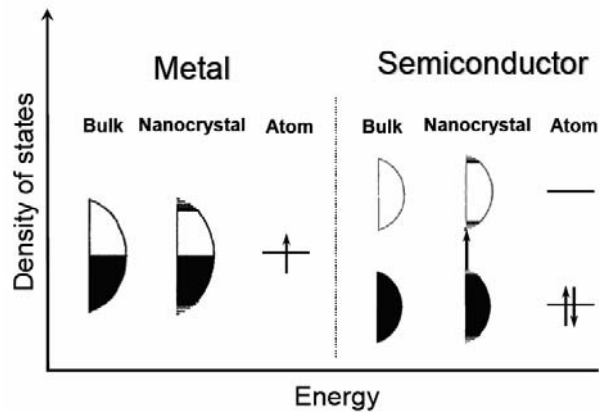


Figure 1.2 Schematic illustration of the density of states in metal and semiconductor clusters.⁵

properties. On one hand, in nanocrystals, the number of surface atoms is in a large fraction of the total, namely the surface-to-volume ratio is drastically increased as the size is decreased. On the other hand, intrinsic properties of the interior of nanocrystals are transformed from classical regime to the quantum size effects. Independent of the large number of surface atoms, semiconductor nanocrystals with the same interior bonding geometry as a known bulk phase often exhibit strong variations in their optical and electrical properties with respect to size.^{3,4} These changes arise from systematic transformations in the density of electronic energy levels as a function of the size of the interior, known as quantum size effects. As depicted in Figure 1.2, nanocrystals lie in between the atomic and molecular limit of discrete density of electronic states and the extended crystalline limit of continuous bands.^{5,6} During the past two decades, the ability to control the surfaces of semiconductors with near atomic precision has led to gain detailed insights into the semiconductor structures: quantum wells, wires, and dots. Neglecting for a moment the atomic level structure of the material, it is possible to imagine simple geometric objects of differing dimensionality in a degree of freedom of two, one, and zero, each case being made out of homogeneous semiconductor material and with perfect surface termination. Such structures should exhibit idealized variations in density of electronic states predicted by simple “particle in a box” type models of elementary quantum mechanics,

with the continuous levels of the 3D case evolving into a discrete state of the zero-dimensional case (Figure 1.3). Recently, substantial progresses have been made in the preparation and

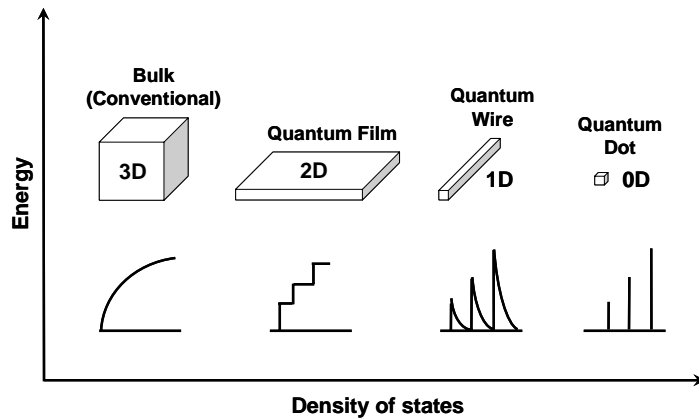


Figure 1.3 Idealized density of states for one band of a semiconductor structure of 3, 2, 1, and “0” dimensions. (In the 3d case the energy levels are continuous, while in the “0d” or molecular limit the levels are discrete)^{7b}

characterization of materials consisting zero-dimensional quantum dots, particles with dimensions in the order of a few nanometers called “nanocrystalline materials”⁵⁻¹³

One factor driving the current interest in nanoparticle research is the urgent need for the further miniaturization of both optical and electronic devices.^{14,15} There exist practical constraints associated with current technologies; due to the diffraction limit, at current stage, lithographic methods cannot be used with a resolution much less than ca. 50 nm. Thus, bottom-up process is indispensable in improving the miniaturization. On the other hand, most semiconducting materials, such as the II–VI or III–VI semiconductors, show quantum confinement behavior in the 1–20 nm size range, depending on the Bohr radius, a size smaller than what can be achieved using present lithographic methods. Thus, their associated fundamental properties and perspectives in application are unprecedented. In view of these challenges, the motive of this research will focus on the study of II-VI semiconductor QDs.

1.1. Theoretical considerations of bulk and nanocrystalline semiconductors¹⁶

Typically, 1–20 nm size range semiconductor nanocrystallites show optical, electronic, and mechanical properties distinctly different from those of the corresponding bulk material elaborated as follows.

1.1.1. Bulk semiconductors

Macrocrystalline semiconductors, if they are free of defects, consist of three-dimensional networks of ordered atoms. The translational periodicity of the crystal imposes a special form on the electronic wave functions. An electron in the periodic potential field of a crystal can be described using a Bloch type wave function (eq. 1), where $u(r)$ represents a Bloch function modulating the plane wave $\phi(kr)$ of wave vector \mathbf{k} .

$$\psi(r) = \phi(kr)u(r) \quad (1)$$

$$u(r+n) = u(r) \quad n \text{ integer} \quad (2)$$

In a bulk semiconductor, the large number of atoms leads to the generation of sets of molecular orbitals with very similar energies, which effectively form a continuum. At 0 K the lower energy levels, or valence band, are filled with electrons, while the conduction band consisting of the higher energy levels is unoccupied. These two bands are separated by an energy gap (E_g), the magnitude of which is a characteristic property of the bulk macrocrystalline material at a specific temperature. Materials normally considered as semiconductors typically exhibit band gaps in the range of 0.3–3.8 eV, covering an optical response from UV-Vis to higher energy side of the infrared region.

At temperatures above 0 K, electrons in the valence band may receive enough thermal energy to be excited across the band gap into the conduction band. An excited electron in the conduction band, together with the resulting hole in the valence band, forms an “electron-hole pair”. The conductivity (σ) of the semiconductor is governed

by the number of electron-hole pairs, the charge carrier concentration (n , normally expressed in terms of the number of particles per cubic centimeter), and their mobility (μ). Thus conductivity can be expressed as the sum of the electrical conductivities of electrons and holes expressed in eq. 3, in which q denotes the charge of carrier. In conventional semiconductors, electrons and holes are the charge carriers. At ambient temperature, they exist in small numbers as compared to those of the conductors. However, it should be noted that the carrier mobilities in semiconductors are substantially larger than that in many conductors.

$$\sigma = qn_e\mu_e + qn_h\mu_h \quad (3)$$

The charge carriers in a semiconductor can form a bound state when they approach each other in space. This bound electron-hole pair, known as a Wannier exciton, is delocalized within the crystal lattice and experiences a screened Coulombic interaction. The Bohr radius of the bulk exciton is given in eq. 4 expressed as

$$a_B = \frac{\hbar^2 \varepsilon}{e^2} \left[\frac{1}{m_e^*} + \frac{1}{m_h^*} \right] \quad (4)$$

where ε represents the bulk optical dielectric coefficient, e the elementary charge, and m_e^* and m_h^* the effective mass of the electron and hole, respectively.

1.1.2. Nanocrystalline semiconductors

Two fundamental factors, both related to the size of the individual nanocrystal, distinguish their behavior from the corresponding macrocrystalline material. The first is the high dispersity (large surface/volume ratio, vide supra) associated with the particles, with both the physical and chemical properties of the semiconductor being particularly sensitive to the surface structure. The second factor is the actual size of the particle, which can determine the electronic and physical properties of the material.

The absorption and scattering of incident light in larger colloidal particles can be described by Mie's theory. However the optical spectra of nanocrystalline compound semiconductors⁵⁻¹³ which show blue shifts in their absorption edge as the size of the particle decreases cannot be explained by classical theory.¹⁷⁻²¹ Such size dependent optical properties are examples of the size quantization effect which occurs¹⁷ when the size of the nanoparticle is smaller than the bulk-exciton Bohr radius, a_B (see eq. 4), of the semiconductor. Equation 5 defines, for a spherical crystallite of radius R , the region of intermediate character between that of a "molecule" and that of the bulk material (l is the lattice spacing)

$$l \ll R \leq a_B \quad (5)$$

Charge carriers in semiconductor nanocrystallites are confined within three dimensions by the crystallite. In the case of ideal quantum confinement the wave function in eq. 1 has to satisfy the boundary conditions of

$$\psi(r \geq R) = 0 \quad (6)$$

For nanoparticles the electron and hole are closer together than in the macrocrystalline material, and as such the Coulombic interaction between electron and hole cannot be neglected; they have higher kinetic energy than in the macrocrystalline material. On the basis of the effective mass approximation, Brus showed^{8,19,20} for CdS or CdSe nanocrystallites that the size dependence on the energy of the first electronic transition of the exciton (or the band gap shift with respect to the typical bulk value) can be approximately calculated using

$$\Delta E \cong \frac{\hbar^2 \pi^2}{2R^2} \left[\frac{1}{m_e^*} + \frac{1}{m_h^*} \right] - \frac{1.8e^2}{\epsilon R} \quad (7)$$

Equation 7 is an analytical approximation for the first electronic transition of an exciton, which can be further described by a hydrogenic Hamiltonian,

$$\hat{H} = \frac{-\hbar^2}{2m_e^*} \nabla_e^2 - \frac{\hbar^2}{2m_h^*} \nabla_h^2 - \frac{e^2}{\epsilon |r_e - r_h|} \quad (8)$$

In eq. 7 the Coulomb term shifts the first excited electronic state to lower energy, R^{-1} , while the quantum localization terms shift the state to higher energy, R^{-2} . Consequently, the first excitonic transition (or band gap) increases in energy with decreasing particle diameter. This prediction has been confirmed experimentally for a wide range of semiconductor nanocrystallites,⁵⁻¹³ with a blue shift in the onset of the absorption of light being observed with decreasing particle diameter. Moreover, the *valence* and *conduction bands* in nanocrystalline materials consist of discrete sets of electronic levels and can be viewed as a state of matter between that of molecular and the bulk material.

Equation 7 does not account for a number of other important effects observed in real nanocrystallites,²¹ such as the coupling of electronic states and effects attributable to surface structure. Especially, the constants used in the model (the effective masses and the dielectric constants) are those for macrocrystalline solids. The model is not quantitatively accurate and the corresponding calculations deviate from experimental values, especially for nanocrystallites with a very small size. In such particles the first electronic transition is located in a region of the energy band, in which the normal effective mass approximation is not valid. Although eq. 7 is not valid for all types of semiconductors, from a practical point of view, this model is particularly useful and the size-dependent energy shift for a number of nanocrystalline semiconductors can be qualitatively estimated. Furthermore, the model also provides a fundamental understanding of the quantum confinement effects observed in semiconductor nanocrystallites.

1.2 Reviews of the Applications to Semiconductor QDs

Certainly, various applications of semiconductor QDs have been reported. Some representatives are introduced as follows.

1.2.1 Applications of Devices

In addition to the bio-labeling in the application of QDs, because of its unique optical as well as highly luminescent properties, nanocrystalline could be applied in light-emitting diodes (LEDs),²²⁻²⁷ photovoltaic solar cell,²⁸⁻³² and multicolor lasing.³³⁻⁴⁵

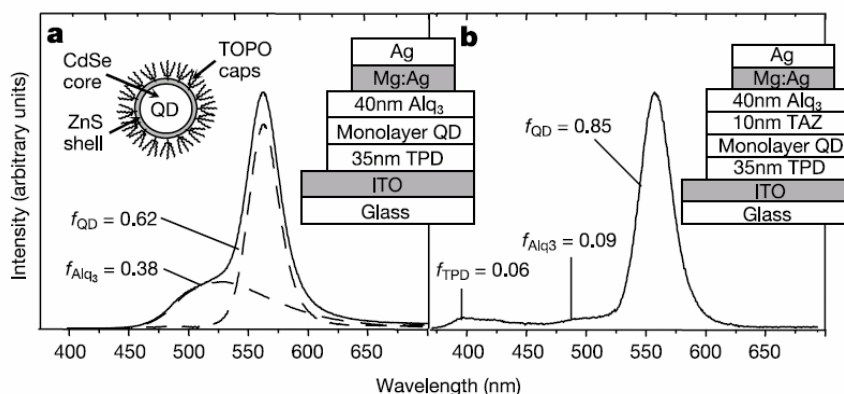


Figure 1.4 Electroluminescence from single monolayers of nanocrystals in molecular organic devices.²⁷

Vladimir Bulovic et al.²⁷ demonstrated a quantum-dot LED (QD-LED) that combines the processability of organic materials with the narrow-band, efficient luminescence of colloidal quantum dots (QDs) (Figure 1.4) and observed a

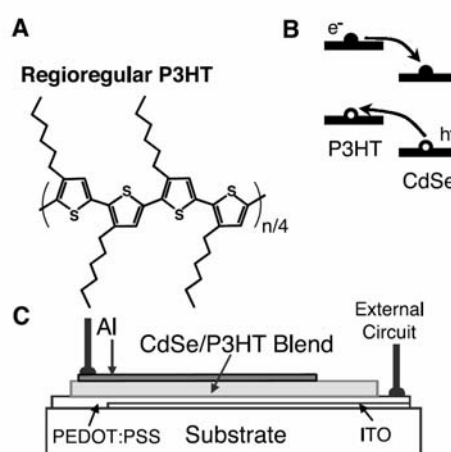


Figure 1.5 Hybrid Nanorod-Polymer Solar Cells³⁰

25-fold improvement in luminescence efficiency over the best previous QD-LED

results.

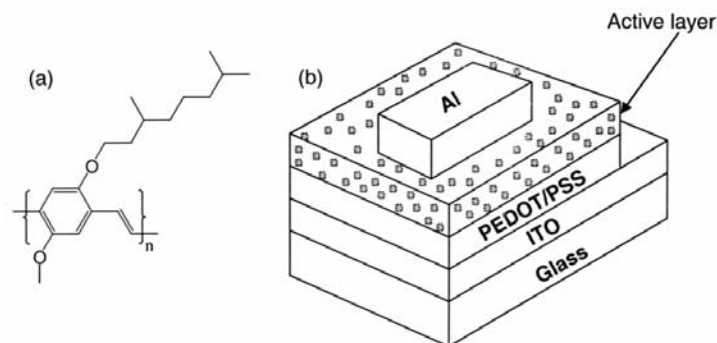


Figure 1.6 (a) Chemical structure of OC₁C₁₀-PPV. (b) Photovoltaic device structure.³¹

As the hybrid solar cells with semiconductor nanorods and polymers (Figure 1.4) fabricated by A. Paul Alivisatos et al.³⁰ in 2002 was arrived a power conversion efficiency of 1.7%, under Air Mass (A.M.) 1.5 Global solar conditions. Neil C. Greenham et al.³¹, the next year, using OC₁C₁₀-PPV to substitute P3HT improved electron transport perpendicular to the plane of the film. Solar power conversion efficiencies of 1.8% were achieved under AM1.5 illumination. (Figure 1.6)

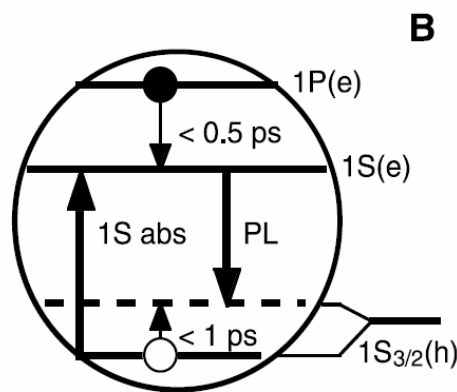


Figure 1.7 Schematics of “absorbing” and “emitting” transitions in CdSe QDs along with intraband relaxation processes leading to a population buildup of the “emitting” transition.³³

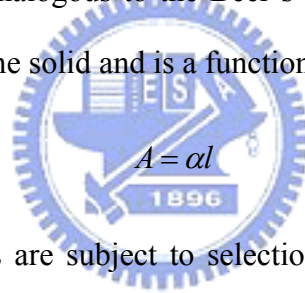
Five years ago, M. G. Bawendi and his co-workers³³ had demonstrated the feasibility of nanocrystal quantum dot lasers. (Figure 1.7)

1.2.2. Optical Properties of Nano-Semiconductor

Quantum size effects have been observed experimentally for many nanocrystalline semiconductors.⁵⁻¹³ The optical absorption spectrum of a

nanocrystalline semiconductor provides an accessible and straightforward method for the evaluation of quantum size effects. The absorption of a photon, leading to excitation of an electron from the valence band to the conduction band, is associated with the band gap energy (E_g). The absorption of photons with energy similar to that of the band gap, $h\nu \geq E_g$, leads to an optical transition, producing an electron in the conduction band of the semiconductor along with a hole in the valence band. Absorption of photons with energy much greater than E_g leads to excitations above the conduction band edge; these electrons can lose the excess energy by radiationless processes.

The absorption (A) of light by a semiconductor material with thickness l can be expressed by an expression analogous to the Beer's law (eq. 9), where R represents the absorption coefficient of the solid and is a function of the radiation frequency.



$$A = \alpha l \quad (9)$$

All electronic transitions are subject to selection rules; for semiconductors the requirements besides the fulfillment of $h\nu \geq E_g$ is that the wave vector, \mathbf{k} , should be conserved. $\mathbf{k}_{\text{photon}}$ is small when compared with the wave vectors of the electron before (\mathbf{k}_e) and after excitation (\mathbf{k}'_e).

$$\mathbf{k}_e + \mathbf{k}_{\text{photon}} = \mathbf{k}'_e \quad (10)$$

$$\mathbf{k}_e = \mathbf{k}'_e \quad (11)$$

The absorption coefficient for a photon of a given energy is proportional to the probability (P_{if}), the density of states in the initial state (n_i), and the density of available final states (n_f). This process must be summed for all possible transitions between states separated by an energy difference equal to the energy of the incident photon.

$$\alpha(h\nu) \propto \sum P_{if} n_i n_f \quad (12)$$

Semiconductors in which there is conservation of the wave vector for optical transitions are referred to as direct band gap semiconductors (see Figure 1.8a) and have large absorption coefficients. A useful expression relating the absorption coefficient and the photon energy of a direct transition near the threshold⁴⁶ is given by eq 13. Semiconductors where the lowest electronic transition, between the valence band and the conduction band, is formally forbidden are said to have an indirect band gap (Figure 1.4b) and normally have small absorption coefficients.

$$\alpha(h\nu) \propto (E_g - h\nu)^{1/2} \quad (13)$$

The “band gap” energy of a nanocrystalline semiconductor can be experimentally estimated from its optical spectrum and by using eq 13. Experimentally, quantum size effects are observed as a shift toward higher energy values for the band edge (a blue shift), as compared to the typical value for the corresponding macrocrystalline material. Nanocrystalline samples often show a peak(s) in the optical spectra at room temperature. It is noticeable that the oscillator strength (directly proportional to the absorption coefficient) increases as the particle size decreases, due to strong overlapping of the wave functions of the confined charge carriers.⁵⁻¹³

In the studies of luminescence II–VI compound semiconductor, monodispersed

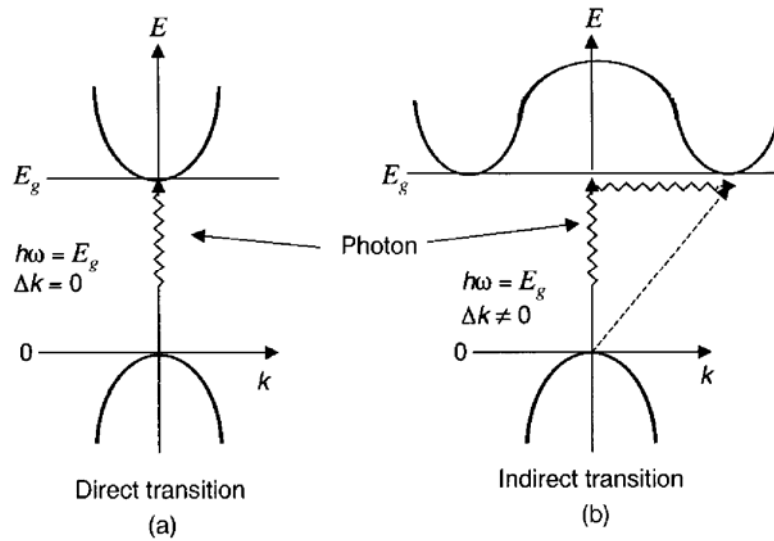


Figure 1.8 Excitation across the band gap by photon absorption: (a) direct process; (b) indirect process.

systems have focused mainly on CdS and CdSe.^{47,48} Cadmium selenide is of interest since light emission can range across the visible region simply by varying the mean diameter of the nanocrystals. As a result, herein, we also would like to focus on the luminescent CdSe nanocrystalline and their applications in both introductory and experimental sections.

1.2.3. Semiconductor QDs as Biological Imaging Agents

Luminescent semiconductor nanocrystal (normally called “quantum dots, QDs” in this thesis) was combination and made by different element in periodic table e.g. IIB–VIA (CdS, CdSe, CdTe, ZnS, ZnTe...etc.) or IIIA-VA (InAs, InP, InN, GaN, GaP, GaAs...etc.), especially CdSe have recently been wildly synthesized and used as labels for bioanalytical application. Their optical properties have significant advantages compared with the organic fluorophores frequently used. Nanocrystals possess high brightness (product of extinction coefficient and quantum yield), with the emission peak wavelength continuously tunable because of quantum size effects. Despite of their broad absorption characteristic, the corresponding emission generally

reveals a narrow spectral line width (which typical full width half maxima (fwhm) of 25~35 nm), and they do not suffer from photobleaching. Many labeling experiments can therefore be performed with luminescent nanocrystals, which are not possible with organic dye, e.g. multicolor labeling with a minimal set of filters, long-term monitoring of dynamic processes, bleach-free scanning confocal fluorescence microscopy, and others.

The pioneers of this approach were started out in 1998 when Chan and Nie, and

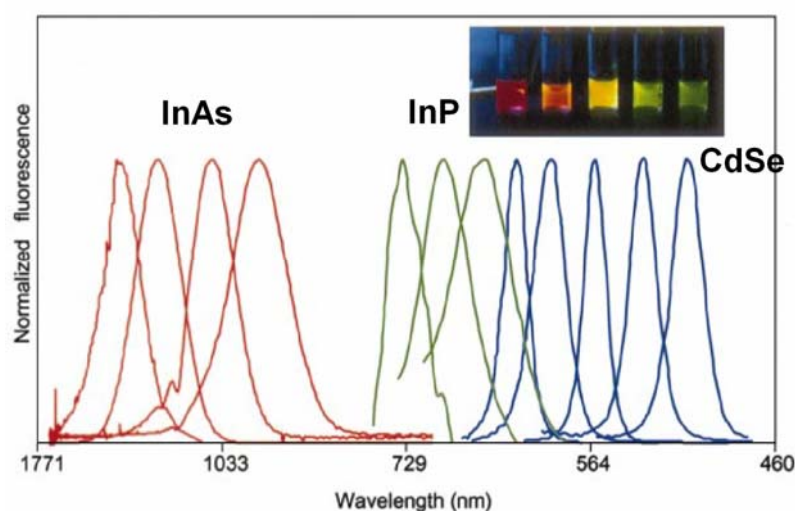


Figure 1.9 Size- and materials-dependent emission spectra of several surfactant-coated semiconductor nanocrystals in a variety of sizes.⁴⁹

Alivisatos et al. published the seminal papers on quantum dots (QDs) bioimaging sequentially.⁴⁹⁻⁵¹ The key factor in using QDs grown in organic solvents was the successful phase transfer to water with minimal loss of emission, while maintaining a bioactive surface. In the researched of Alivisatos and co-worker, they approached the problem by growing three layer of silica (SiO_2) shell around CdSe@ZnS nanoparticles that makes CdSe@ZnS QDs water soluble (Figure 1.9), and used silica chemistry to couple ligands to the shell, which were then utilized in coupling reaction. The resulting materials (which could be engineered to have a maximum quantum yield of 21 %) were used to label mouse fibroblasts (Figure 1.10).^{49,50} The labels

appeared photostable when compared to conventional dyes. Constant excitation of bioactive QDs over 4 h with a 488 nm Argon ion laser resulted in constant emission intensity. In contrast, Rhodamine 6G dyes bleached in 10 mins under identical experimental condition.



Figure 1.10 Mouse 3T3 Fibro-plast labeled with color- tunable QDs.⁵⁰

Subsequently, Chan and Nie applied a simpler method for making CdSe@ZnS nanoparticles water-soluble and bioactive.⁵¹ Solution exchange of the organic ligands on the QDs surface for mercaptoacetic acid (MA) resulted in soluble nanoparticles that have a pendant carboxylic acid group for coupling. They also reported the observation of receptor-mediated endocytosis of the luminescent particles when incubated with HeLa cells (Figure 1.11). Further experiments with immunoglobulin G-QDs conjugated incubated with bovine serum albumin (BSA) and a specific polyclonal antibody demonstrated a tendency for the dots to aggregate when the antibody recognized the so-called fab fragment of the immunoglobulin G. Ever since these two papers have been the basis of numerous relevant studies.

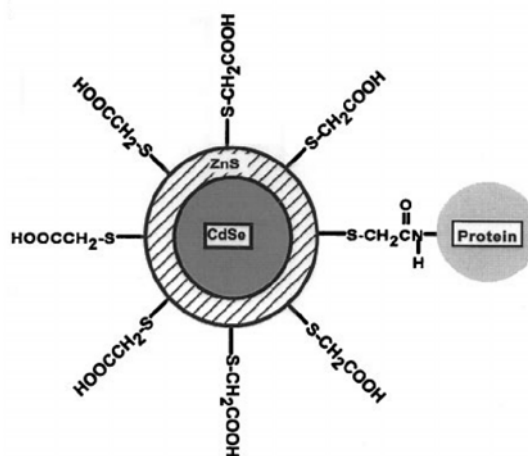


Figure 1.11 ZnS-capped CdSe QDs that is covalently coupled to a protein by mercaptoacetic acid.⁵¹

In one approach, DNA is the ideal synthon for programming the assembly of nanoscale building blocks into periodic two- and three-dimensional extended structures. On the Mitchell and co-worker's approach in 1999, it could be utilized

effectively to guide the construction of macroscopic network assemblies of not only Au nanoparticles⁵²⁻⁵⁶ but also successfully in luminescent QDs.⁵⁷ In their study, Citrate-stabilized gold nanoparticles are ideally suited for direct surface substitution reactions, since the citrate-Au interaction is relatively weak. In comparison to this, modification of QDs with DNA has proven to be much more difficult than for gold nanoparticles. Alternatively, alkylthio functionalized DNA can be used to replace surface bound citrate to generate stable particles with surface bound oligonucleotides susceptible to hybridization with complementary oligonucleotides or particles. The synthetic strategy was shown in Figure 1.12. Another approach for linking biomolecules was reported by Orden and co-workers⁵⁸ in 2001, they also investigated CdSe@ZnS QDs conjugate biotinylated bovine serum albumin (bBSA) and tetramethylrhodamine-labeled streptavidin (SAv-TMR), and observed enhancing TMR fluorescence caused by fluorescence resonance energy transfer (FRET) from the QDs donors to the TMR acceptors (Figure 1.13).

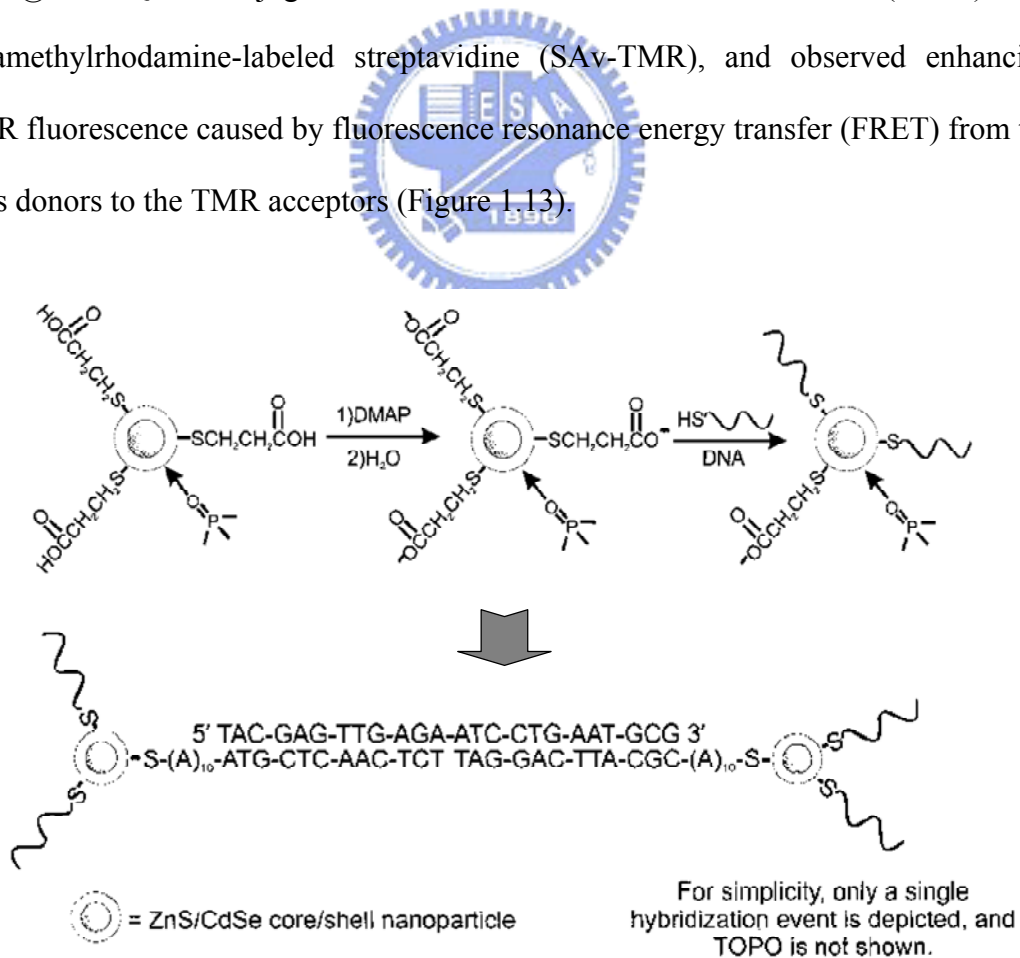


Figure 1.12 The generation of DNA-linked QDs assemblies.⁵⁸

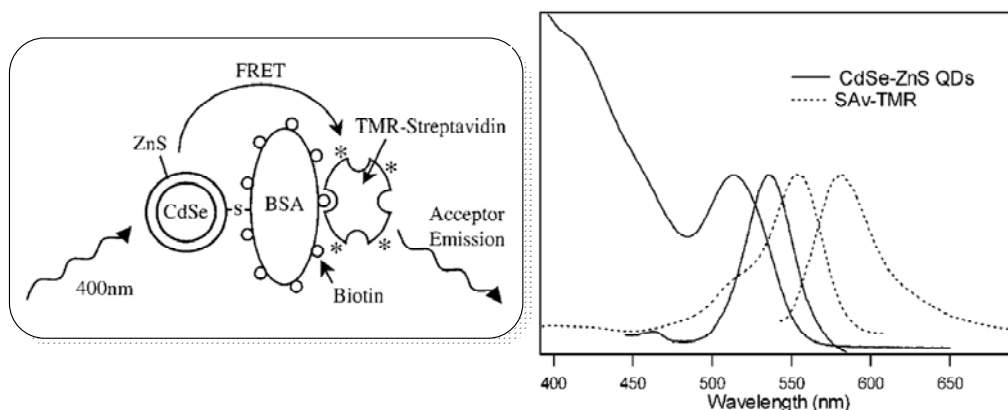


Figure 1.13 Schematic of the FRET binding assay mechanism and normalized absorption and emission spectra.⁵⁸

Phagokinetic track studies into the motility of human mammary epithelial tumor cells and nontumor cells were undertaken in 2002 by Parak et al.⁵⁹ In this approach, thin layers of silica capped CdSe@ZnS were deposited on collagen coated substrates, followed by the plating of cells. Traditional dyes cannot be used owing to photobleaching, while large submicrometer gold particles used previously interfered with cell motility. As a cell passed through the substrate, the uptake of the luminescent cells as a function of time was observed with the confocal fluorescence microscopy. In less than 3h, the tumor cells engulfed nanocrystals, which then clustered in the cytoplasm, presumably in the vesicles. Further experiments revealed that nanoparticles were restricted to the cytoplasm and had not entered the nucleus.

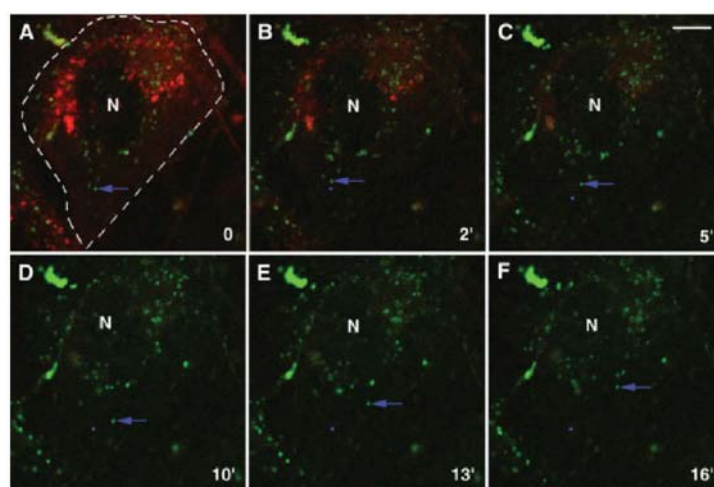


Figure 1.14 Uptake and transport of QDs by breast tumor cells using confocal microscopy.⁵⁹

The migratory pathways of the tumor cells could be differentiated by imaging the substrate and observing areas free of nanocrystals, as a result of the uptake. Imaging of substrates plated with noncancer cells (non-migratory) revealed an intact layer with little evidence of motility. These results confirmed cancer cells are both invasive and migratory, whilst noncancer cells are non-invasive and relatively immotile (Figure 1.14).

One salient remark should be pointed out is that Chan and co-worker in 2002 demonstrated water soluble, biocompatible and color-tunable QDs successfully applied for the biotechnology and bioengineering.⁶⁰ Their approach also employed CdSe@ZnS as QDs and varying the emission color by tuning the QDs particles size (Figure 1.15, up). In addition, they improved the bioconjugation methods via various chemical modifications: (a) use of a bifunctional ligand such as mercaptoacetic acid for linking QDs to biomolecules via a stable amide bond formation (b) TOPO-capped QDs bound to a modified acrylic acid polymer by hydrophobic force (c) QDs

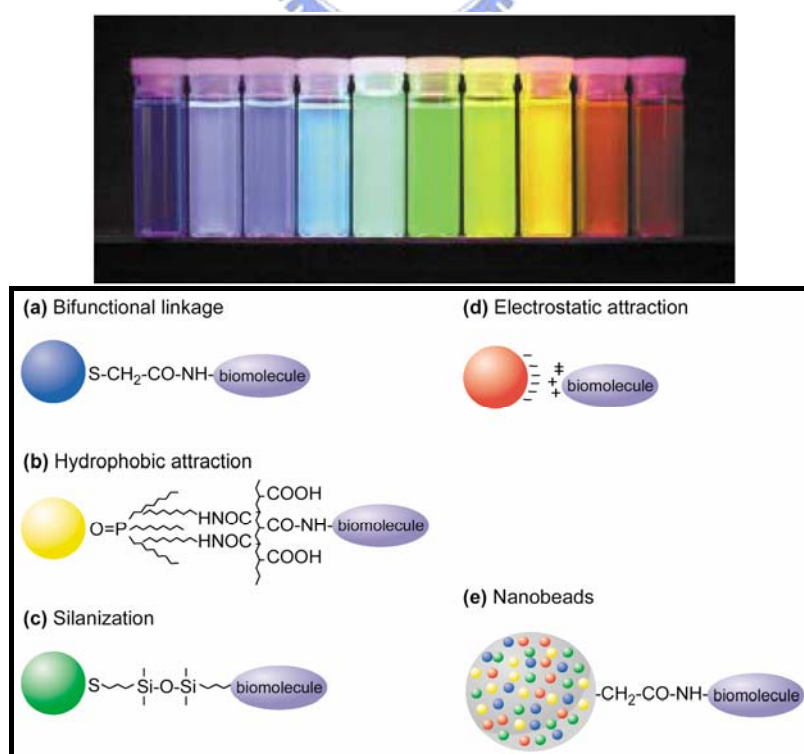


Figure 1.15 (Up) the distinguishable emission colors of CdSe@ZnS QDs excited with a near-UV lamp; (down) schematic illustration of bioconjugation methods.⁶⁰

solubilization and bioconjugation using a mercaptosilan compound (d) positively charged biomolecules are linked to negatively charged QDs by electrostatic attraction (details will be elaborated throughout the thesis) (e) incorporation of QDs in microbeads and nanobeads. (Figure 1.15, down).

One of the first papers describing in vivo studies using QDs are based on mercaptoacetic acid capped CdSe@ZnS, which were then incubated with thiolated peptides. This protocol of passivating the QDs surface was published by Åkerman et

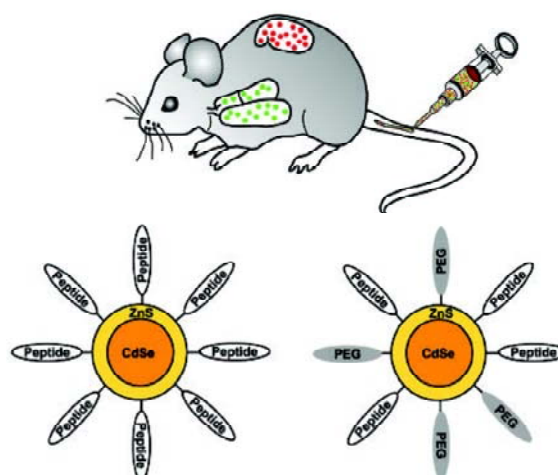


Figure 1.16 Design of QDs coated with either peptides only or with peptides and PEG, then intravenous delivery of this QDs into specific tissues of the mouse.⁶¹

al.⁶¹ Three specific peptides were used in this approach, peptide CGFECVRQCPERC (GFE), which binds to a membrane dipeptidase on the endothelial cells in lung blood vessels; F3, which binds to blood vessels and tumor cells in certain tumors; and LyP-1, which binds to lymphatic vessels and tumor cells in certain tumors. QDs coupled to F3 alone displayed a tendency to aggregate, which was overcome by co-passivating with thiolated polyethylene glycol (PEG) that is known to minimize molecular interactions, improving colloidal stability, and inhibiting nonspecific binding. The QDs were then injected into the tail veins of specifically xenografted mice and left to circulate for up to 20 minutes before the relevant tissues were harvested. As hypothesized, dots passivated with GFE were found in the lungs, and dots capped with F3 and LyP-1 was found in the targeted tumors, whilst the subcellular fluorescence pattern suggested the dots were internalized into the cells. GFE capped

dots were not detected in tumors. The dots were not found in the brain, heart, kidney, or skin, but were observed in the liver and spleen regardless of the peptide used, except when co-passivated with PEG, which reduced co-adsorption by 95% (Figure 1.16). Despite the above applications, there are still problems using specifically capped QDs as biolabels. Simple surface-capping-agent exchange as described by Chan and Nie⁵¹ results in a material with decreased emission efficiency and poor colloidal stability.

Growing a silica shell on the particles as described by Alivisatos et al.⁵⁰ results in a stable material, but is difficult to do, hard to control and a time consuming process. For either method, an important problem for the QDs biolabels to be addressed is the tendency of nonspecific adsorption and aggregation when taken up by cells. Various researchers have addressed these issues, and the improving methods include the addition of small polymeric species on the surface of silica capped QDs, or the use of electrostatic interactions to absorb a protein on the QDs surface which can act as a bridging agent.

In 2002, Dubertret et al. reported a simple way of making bioactive quantum dots that overcome the obstacle of nonspecific binding. In this approach, nanoparticles were encapsulated by phospholipid micelles, so that the outer layer is repellent to biomolecules.⁶² DNA was then coupled to the end of the outer-layer of the micelle, providing a binding point for

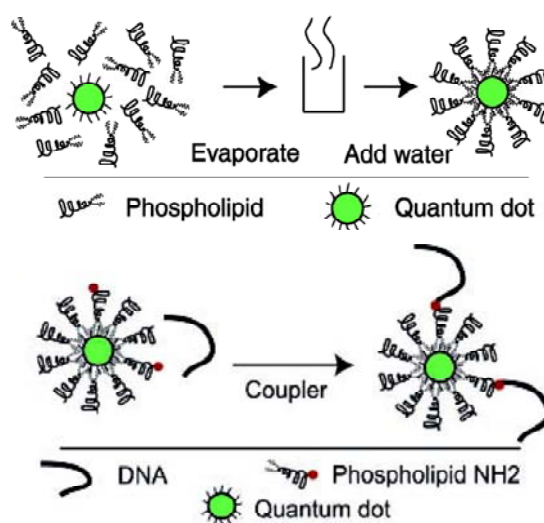


Figure 1.17 Schematic of single-QDs encapsulation in a phospholipids block-copolymer micelle and QDs-micelle conjugation with single-stranded DNA (ssDNA).⁶²

bioconjugation by hybridization. Ideally, the dots need to be slightly bigger than the core, stabilizing the micelle. If the particles are too small, the stability of the micelle is affected and multiple dots can inhabit a single cavity. Simple QDs micelles were injected into *Xenopus* embryos and used in vivo studies. The micelles appeared to be cell autonomous, had little toxic effect on the cells and were stable in vivo showing no signs of aggregation after 4 days. The micelles were used to successfully label numerous cell types, and remained luminescent throughout embryonic development despite pigmentation and background fluorescence (Figure 1.17).

In another approach, deep tissue in vivo imaging and blood-flow monitoring studies were also carried out by Webb and co-workers in 2003 using CdSe@ZnS capped with an octylamine modified polyacrylic acid.⁶³ The probes were determined to have two-photon action cross sections (a measure of brightness for imaging) of up to 47000 Goeppert–Mayer (GM) units, an order of magnitude higher than organic molecules designed for similar biological functions and close to the theoretical maximum for CdSe dots, estimated at 50000 GM. The dots appeared stable for months and the action cross-section remained constant, however, a large fraction of nonfluorescent dots were also observed. No evidence for blinking (fluctuation of

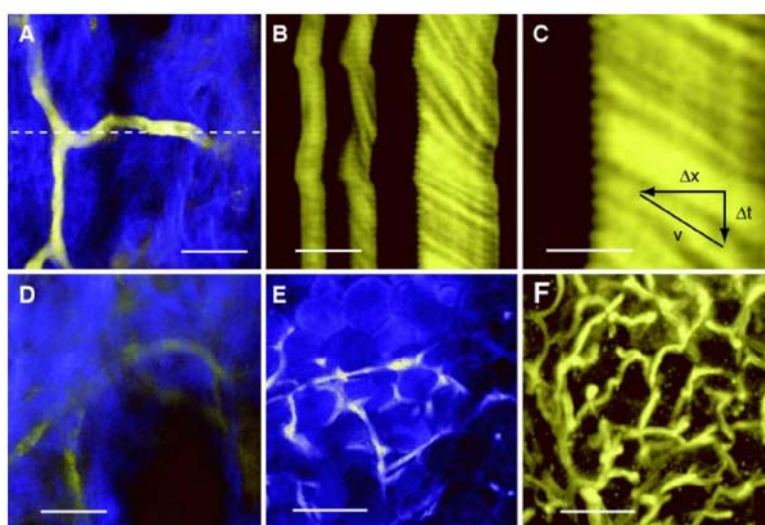


Figure 1.18 Deep tissue imaging of a vasculature system.⁶³

radiation intensity) was observed and it is suggested that this phenomenon averages out and is unlikely to be an issue in nanoparticle imaging applications. It was observed that the sizes of the quantum dots are similar to fluorescent dextrans, which make them ideal for angiography. Intravenous injection in live mice was also carried out to examine skin and adipose tissues, both of which are highly scattering and have a high refractive index mismatch. The vasculature system was clearly observed through unbroken skin up to 250 mm deep. Compared to similar imaging agents such as fluorescent dextrans (compare Figure 1.18 a and d), quantum dots shows significantly clear image with less power, attributable to the high action cross-section. Figure 1.18 shows images obtained from the study, highlighting various structures (the blue color is collagen autofluorescence). The mice used in the study showed no ill effects from the cadmium-containing labels and investigations are ongoing as to the suitability of heavy-metal containing labels.

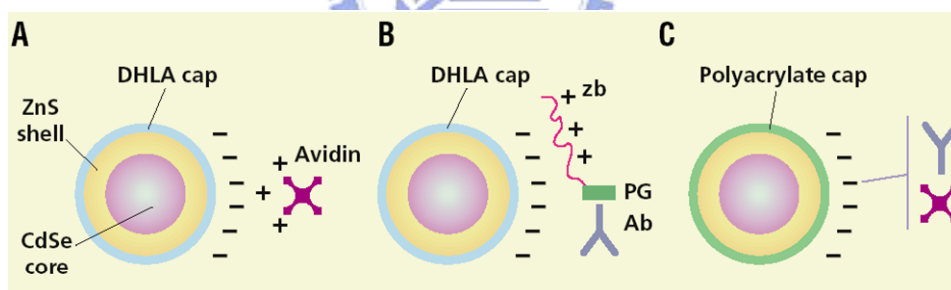


Figure 1.19 Three strategies for bioconjugation to QDs probe.

Semiconductor quantum dots are becoming highly efficient tools for biological imaging and have numerous demonstrated advantages over conventional dyes. Other studies of note include the imaging of the cancer marker Her2, live cells, performed by Wu et al.⁶⁴ and Jaiswal et al.⁶⁵ respectively in 2003 (see Figure 1.19), the QDs consists of a CdSe core passivated by a ZnS shell. The surface cap is negatively charged, with carboxylate groups from either DHLA or an amphiphilic polymer. Proteins are conjugated to the DHLA-QDs electrostatically either (A) directly or (B)

via a bridge consisting of a positively charged leucine zipper peptide (zb) fused to recombinant protein G (PG). The latter binds to a primary antibody (Ab) with specificity for the intended target. In (C), antibodies, streptavidin, or other proteins are coupled covalently to the polyacrylate cap with conventional carbodiimide chemistry. Also, the quantum-dot doped polystyrene beads designed for assays have attracted much attention⁶⁶ (Figure 1.20). The beads are particularly note worthy as they are internalized into the bead core without requiring surface exchange, thus maintaining their luminescent efficiency. The controlled manner, in which this was achieved, allowed for the development of a quantum dots bar based assay.

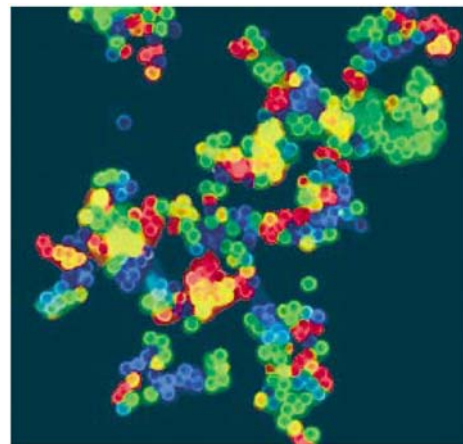


Figure 1.20 Microbead containing various levels of CdSe@ZnS QDs.⁶⁶

Other novel approaches in QDs conjugated to bio-molecules are briefly discussed as follow. In 2001, Mattoussi et al. described a novel approach to the coupling

of biomolecules with semiconductor quantum dots.⁶⁷ They prepared a recombinant protein linker that contained a basic leucine zipper motif, which induces a net positive charge, thereby allowing electrostatic binding to negatively

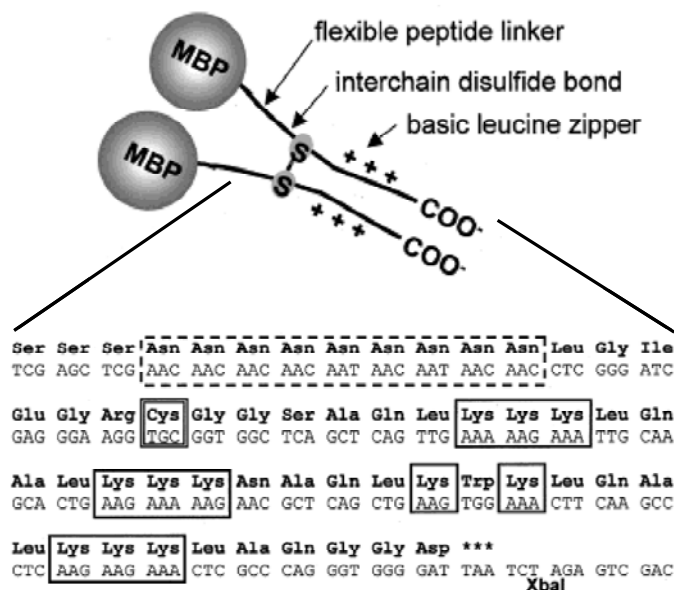


Figure 1.21 Recombinant protein linker contains a functional protein moiety, MBP, and a basic leucine zipper motif.⁶⁷

charged semiconductor QDs (Figure 1.21). Functional proteins, such as bioactive enzymes or binding proteins can be attached to the leucine zipper motif through the flexible linker chain by means of genetic engineering. The use of a model fusion protein, which consists of the maltose binding protein (MBP), allowed the preparation of biofunctionalized 4-nm CdSe@ZnS quantum dots possessing 19 protein molecules per nanoparticle. The conjugates had the full biological functionality of the MBP as well as the undisturbed photoluminescent properties of the quantum dots. Moreover, it was observed that the binding of the leucine zipper is beneficial to the stability of the nanoparticle stability in aqueous solutions. The QDs linkage to biomolecules based on other methods have also been reported.⁶⁸⁻⁷⁵ One who is interested in the relevant subjects can refer to recent review papers.⁷⁶⁻⁸⁰

1.2.4. Exceptional surface modification of quantum dots

In view of QDs surface modification, as elaborated in the previous sections, it is clear that the water-soluble QDs linked biological imaging was prepared mostly by capping with a mercaptocarboxylic acid (HS–RCO₂H) layer, e.g. mercaptoacetic acid (MA), mercaptopropionic acid (MPA), and dihydroxylipoic acid (DHLA) etc.^{51,57,66,71,73,82} The main reason for using thio- (–SH) derivatives as a linkage is that its affinity to QDs was much higher than other functional groups. In addition to this general method, a surface modification without sulfur linkage have recently been developed and is named as the “polymer–coated water soluble QDs”.

For example, Klimov and co-workers have successfully employed hydrophobically modified polymers to solubilize nanoparticle (or QDs).⁸³⁻⁸⁵ Low-molecular weight polyacrylates modified with octyl chains were developed to stabilize and encapsulate QDs, rendering them soluble in polar media e.g. water or alcohol. The amphiphilic polymer encases the nanoparticle, creating a micellar shell

around QDs. The hydrophobic groups are then cross-linked to stabilize the QDs-polymer conjugate for preparing shell cross-linked knedels (SCKs) (Figure 1.22). The exploration not only yields polar solvent soluble QDs but also to manipulate the resulting QDs-polymer complexes into assemblies.

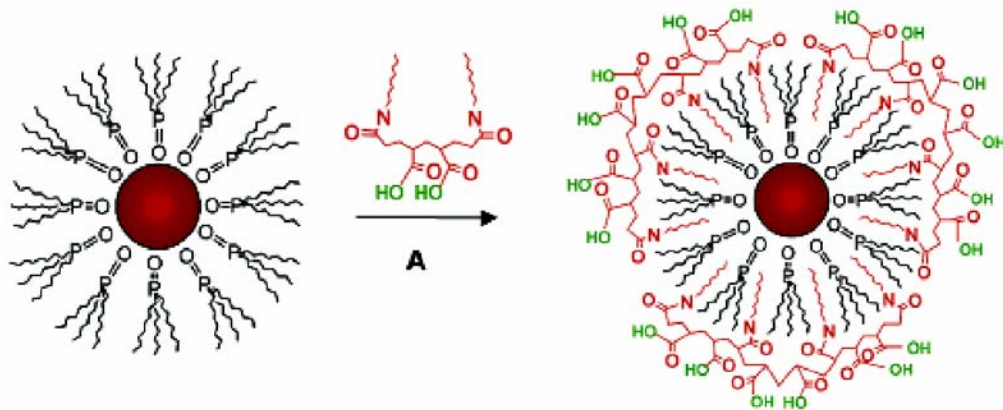


Figure 1.22 Formation of the polymer-QDs showing and idealized micellar polymer shell (40% octylamine- modified PAA) encapsulating the QDs.

Also in 2004, Nie's group developed a polymer coated QDs and applied to *in vivo* cancer targeting.⁸⁶ Because of strong hydrophobic interaction between TOPO and the polymer hydrocarbon, these two layer "bond" (actually not a really chemical bond

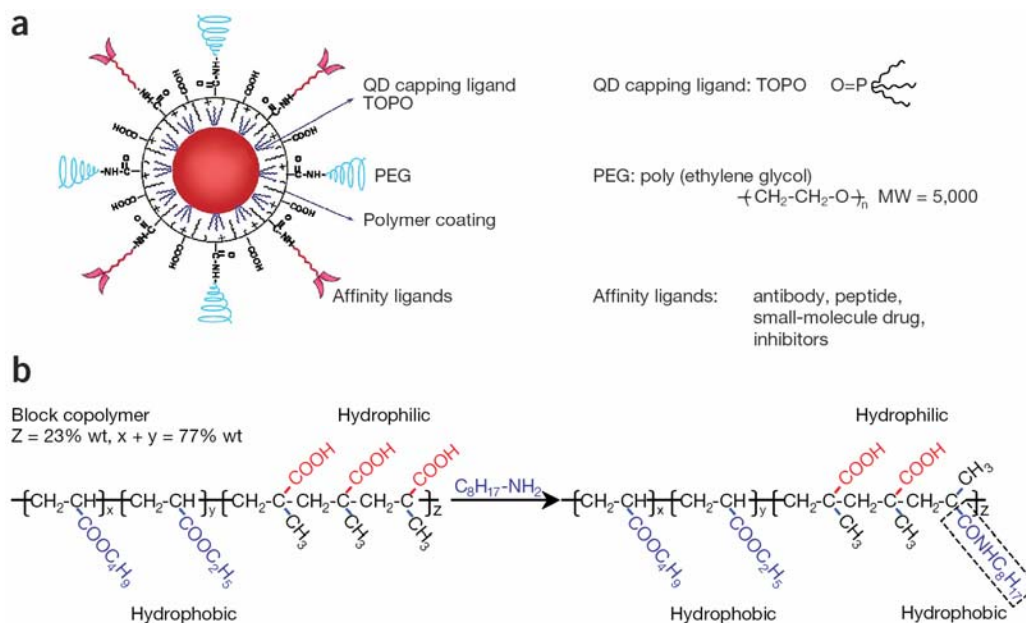


Figure 1.23 Schematic illustration of bioconjugated QDs for on *vivo* cancer targeting by modified polymer on surface.⁸⁶

formation, just an attraction between aliphatic chain) to each other and form a hydrophobic layer. The proposed scheme is depicted in Figure 1.23, consisting of: (a) Structure of a multifunctional QD probe, showing the capping ligand TOPO, an encapsulating copolymer layer, tumor-targeting ligands (such as peptides, antibodies or small molecule inhibitors) and polyethylene glycol (PEG), (b) chemical modification of a triblock copolymer with an 8-carbon side chain. This hydrophobic side chain is directly attached to the hydrophilic acrylic acid segment and interacts strongly with the hydrophobic tails of TOPO. Dynamic light scattering shows a compact QD-polymer structure, indicating that QDs are tightly wrapped by the hydrophobic segments and hydrocarbon side chains. Other laboratories like Zhang et al.⁸⁶ and Pellegrino et al.⁸⁷ also prepared water-soluble polymer-coated QDs only by varying the surface polymer.

Another novel attempted surface modification on QDs is using the concept of electrostatic attraction. Jaffar et al.⁸⁸ reported the modification of CdSe@ZnS QDs surfaces with polyelectrolyte coating layer-by-layer (LbL). Although the first step was modified by mercaptoacetic acid (MAA) on the CdSe@ZnS QDs surfaces, this strategy provides a novel concept to change the electrostatic of the surfaces. Since the surface was fully negatively charged upon modification with MAA, subsequent modification of the surface with positively charged substituents such as polyallyl

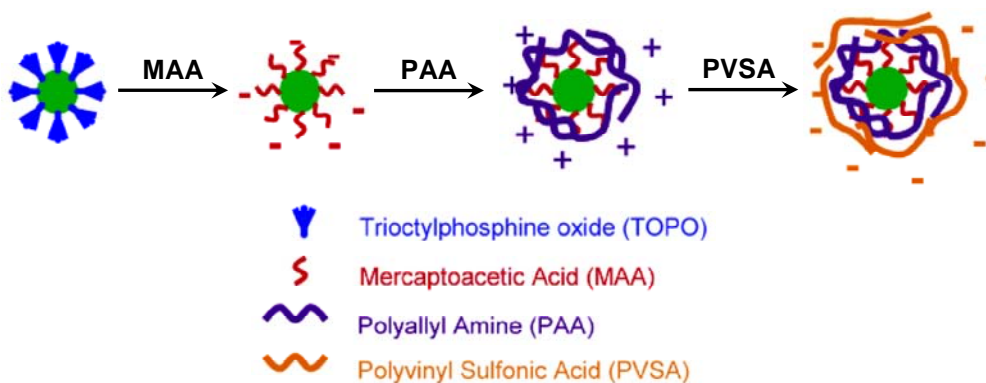


Figure 1.24 QDs surfaces modification and modifying the surface charge arbitrarily by coating different polymer.⁸⁸

amine (PAA, positively charged polymer) are necessary. As a result, they keep on modifying the polyvinyl sulfonic acid (PVSA, negatively charged polymer) to the polymer-coated QDs, followed by reversing the charge alternatively as shown in Figure 1.24.

By the same layer-by-layer (LbL) technique, Hong et al.⁸⁹ went one step further to work on magnetic QDs by changing polymer to polyallylamine hydrochloride (PAH) and polysodium 4-styrenesulfonate (PSS). They also varied the surface charge by fine-tuning negative or positive charge at will.

Of particular interest is the method recently reported by Peng and co-workers,⁹⁰ in which a new strategy, dendrimer bridging, is developed for simultaneous formation and functionalization of

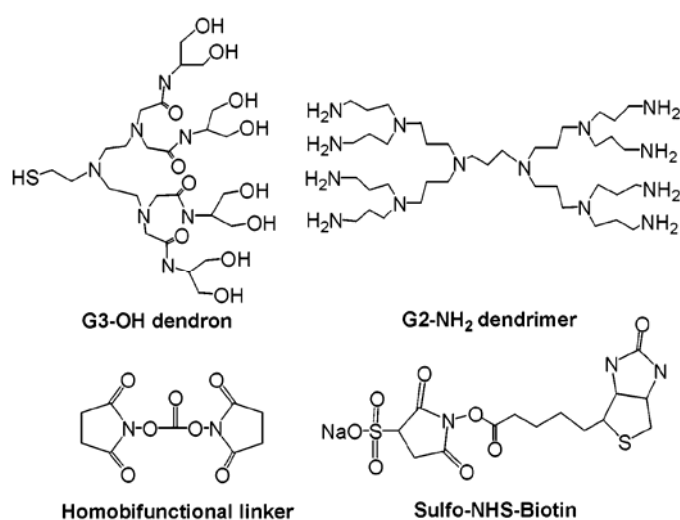


Figure 1.25 Four key compounds used of Peng's work.⁹⁰

biocompatible and bioaccessible CdSe@CdS semiconductor box nanocrystals; namely, a dendron box around each colloidal semiconductor nanocrystal. Apparently, as shown in Figure 1.25, the use of four key compounds as extended linkers constructs the overall framework. In this protocol, CdSe plain core or CdSe@CdS core/shell nanocrystals coated by a monolayer of organic dendron ligands (dendron nanocrystals) with hydroxyl groups as the terminal were chosen as the starting systems because of their potential biocompatibility and stability. A generation-two (G2) aminoterminated dendrimer was then used as the cross-linking and functionalization reagent, which yielded much more stable cross-linked nanocrystals than did the simple diamine or

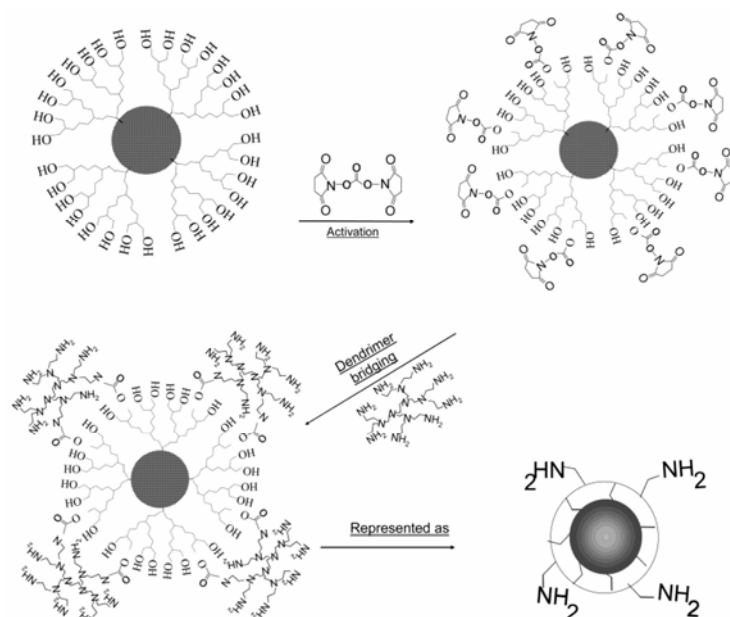


Figure 1.26 One-pot formation of amine box nanocrystals.⁹¹

trisamine cross-linking reagents. The chemical, thermal, and photochemical stability of the resulting amine-terminating box nanocrystals (amine box nanocrystals) formed by dendrimer bridging are comparable to that of the first generation box nanocrystals. Note that the first generation box nanocrystals are not biocompatible and need to be further functionalized for bioapplications⁹¹ (Figure 1.26). The amine groups on the surface of the box nanocrystals provide versatile and reliable conjugation chemistry under mild conditions⁹² (Figure 1.27). Using one of the conjugation methods, biotin molecules were readily coupled onto the amine box nanocrystals. The biomedical applications of those superstable box nanocrystals were demonstrated by the quantitative and reproducible precipitation of the picomole amounts of avidin with the biotinylated box nanocrystals.

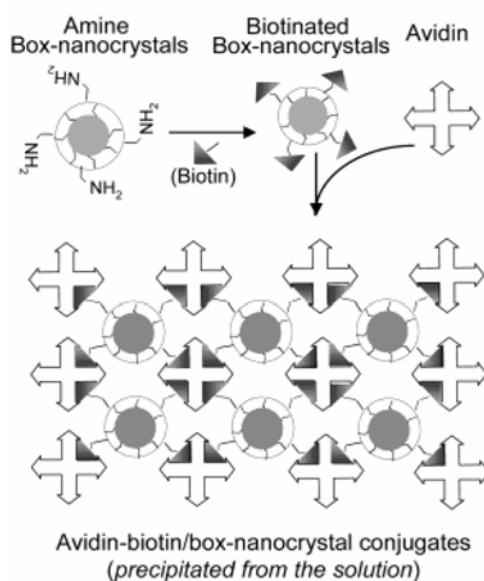


Figure 1.27 Schematic procedure for the formation of avidin-biotin/box nanocrystal conjugates.⁹²

1.3. The Backgrounds of Core/Shell Quantum Dots

1.3.1. Type-I CdSe@ZnS(ZnSe) Core/Shell Quantum Dots

Due to their remarkable size dependent photophysical properties and versatility toward chemical modification (vide supra), semiconductor quantum dots (QDs) have received considerable attention,^{5-13,18-21,89} among which cadmium chalcogenides have been actively playing a role in the relevant

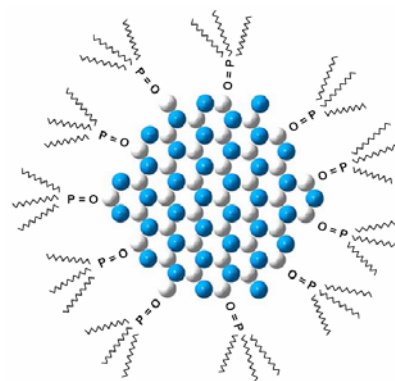


Figure 1.28 Nanocrystal surrounded by TOPO chains anchored to its surface.

II-VI QDs synthesis due to its high luminescence yield, monodispersity, uniform size and shape. Consequently, upon coupling to e.g. bio-molecules, the luminescent QDs may serve as an ultra-sensitive biological probe.³⁷⁻⁶⁵ Numerous synthetic routes have been developed for the preparation of monodispersed cadmium chalcogenide. Herein, I'd like to elaborate a specific one-pot reaction toward modification of the highly luminescent QDs (e.g. CdSe@ZnS). This synthetic route was developed via the collaboration between Professor Chou and our groups. Of particular interest is the reagents incorporated are environmentally safe and much less expensive (vide infra). Prior to this QDs scenario, it is necessary to have brief introduction on notions regarding certain terminologies in this field as well as to review several common synthetic methods recently developed by other contributors.

1.3.1.1. Surface Passivation

Nanocrystals synthesized from liquid-phase epitaxy frequently need a certain surfactant or called “stabilizer” to make the nano-structure stabilized, by capping the surface with surfactant molecules. Normally this is called “organic surface passivation” as shown in Figure 1.28. For example, TOPO (Trioctylphosphine Oxide)

is the very popular ones. However, there is a barrier of steric hindrance and electrostatic repulsion between organic TOPO chain surrounding the QDs surface.

It should be noted that the resulting particle might contain some non-absorbed parts, which are called “unpassivated atoms”. Such imperfect atoms also make stacking fault and become “defects”, which may significantly influence the stability and photophysical properties of QDs. There are two radiative pathways commonly applied for the nanocrystals

excited by photons. As shown in Figure 1.29⁹³, the first one is the band edge emission. The concept of this is the same with the bulk semiconductor, i.e. the emission from electron and hole recombination. The

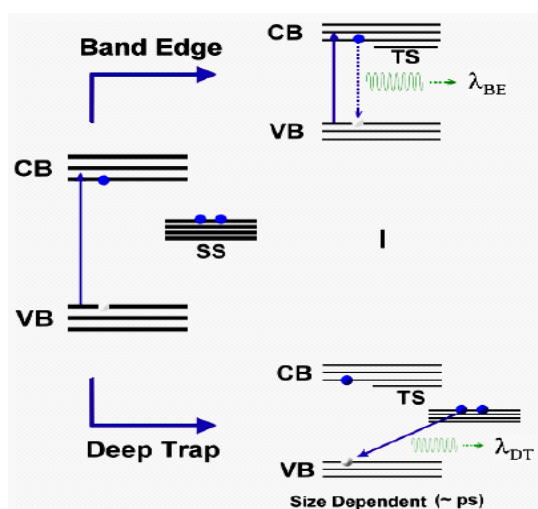


Figure 1.29 Common emission mechanism of the semiconductor nanocrystal.

other one is the deep trap emission. There are additional energy levels commonly called the surface state (SS) originated from bare (or unpassivated) atoms. In the CdSe case, selenium is always considered as the unpassivate atoms because cadmium has higher affinity toward organic surfactant than selenium. This midgap state of the surface could be either electron donor or even electron acceptor. These states strongly affect the emission property as well as reduce the luminescence efficiency. The key factor to synthesize high quality QDs is to control the passivated surface of nanocrystal. In other words, the manipulation of controlled the chemical and physical properties of the particles.

1.3.1.2. Protective Types Core/Shell Structure

Core/shell type composite quantum dots exhibit novel properties. These make them attractive both experimentally and practically. The properties of core/shell QDs are highly dependant on the inorganic surface passivation and obey the principles of quantum well. Previously, Figure 1.28 shows passivation and stabilization of organic surfactant (e.g. TOPO or TOP), on CdSe QDs. Nevertheless, due to imperfect surface passivation and rearrangement of the surface atoms, deficient quantum confinement effect on the surface may takes place. Overcoating nanocrystallites with inorganic materials of higher band offsets has been shown to improve the photo-luminescence quantum yield (QY). This is achieved by passivating surface nonradiative recombination sites. As

illustrated in Figure 1.30, ZnS or CdS shell capped CdSe QDs always provides higher quantum efficiency (QE) and photo stability due to the confinement of the carrier on the edge of the energy band offsets,

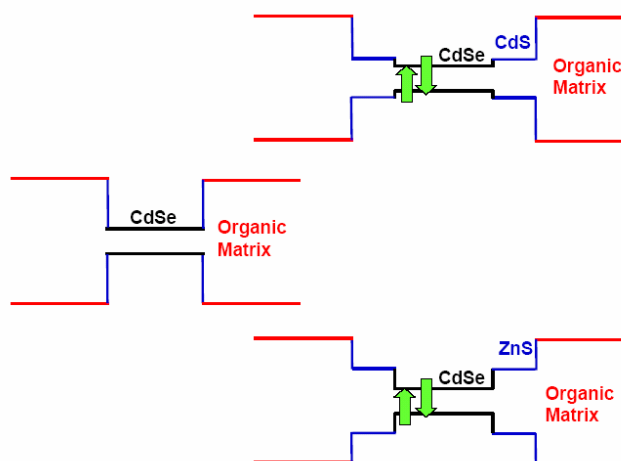


Figure 1.30 Bared CdSe QDs and inorganic surface passivation core/shell type-I QDs.

and consequently reducing the loss of the carrier by trapping or tunneling.⁹⁰⁻⁹² Herein, we call the case as type I core/shell QDs that the valence band of core is higher in energy than that of the shell, while the relative energy level is opposite in the coduction band.

The passivation also increases more protection and stability than the core only and the organically passivated core nanocrystals. The following example⁹⁴ illustrates

the property changes of the core/shell structure. Although the stability was investigated by differentiating the bare (organic TOPO-coated) InAs cores and InAs@CdSe (or InAs@ZnSe) core/shell samples, its suitability should be applied to other QDs. By comparing absorption and emission spectra of the fresh samples and of samples that were kept for 10 months in a solution saturated with oxygen under daylight conditions, the results shown in Figure 1.31 clearly indicate that InAs cores

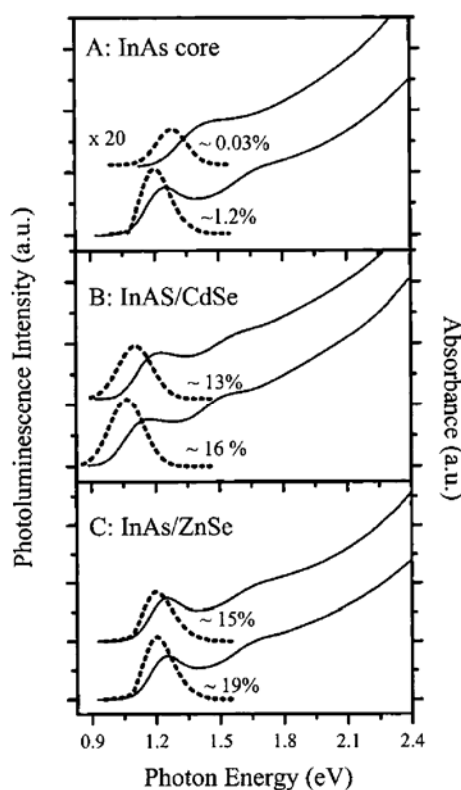


Figure 1.31 Comparison of stability of core and two types of core/shell QDs.⁹⁴

under these conditions exhibited a considerable quenching by a factor of 40 (Figure 1. 31A). These phenomena indicate substantial oxidation of the bare InAs core. The core/shells under similar conditions show a very different behavior. For InAs@CdSe and InAs@ZnSe core/shell QDs the absorption shifted slightly to the blue and the QY decreases from 16 to 13% and 19 to 15% respectively (Figure 1. 31 B, C). Evidently, the photo-stability of the bare QDs is not as great as that of the core/shell type QDs.

Despite the superiority of core/shell QDs, there are certain limitations of applying the shell layers. Particularly, two factors determine the quality of shell passivation. The major

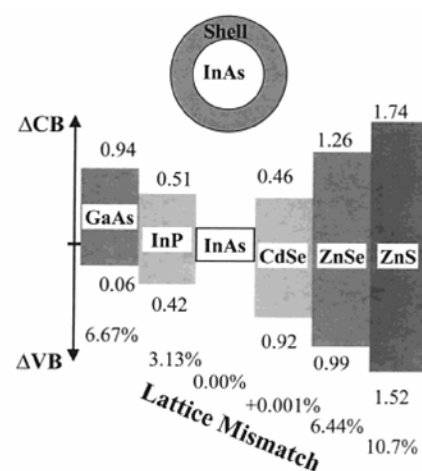


Figure 1.32 Summary of the band offsets (in eV) and lattice mismatch (in %) between the InAs core and other shells.⁹⁴

concern lies in the lattice mismatch between the core and the shell materials. It is important in the synthesis of heterostructure core/shell nanocrystal because extremely large lattice mismatch could enable tension during the shell passivation and eventually result in the collapse or defect of nanocrystallines. As shown in Figure 1.32 the InAs core and the CdSe shell have a minimum lattice mismatch, while there is a mismatch as high as 10.7% between the core and the ZnS shell resulting in the difficulty of growth.⁹⁴ The other major factor is that the shell band offsets should be covering the core one. For example, the band offsets of the CdSe shell caps the InAs core and the ZnSe shell caps the CdSe core (vide infra).

1.3.2 Type-II Core/Shell Quantum Dots

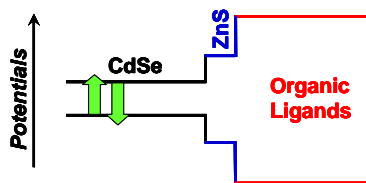
Despite well-documented studies of type-I core/shell semiconductor quantum dots (QDs), studies of type-II QDs are relatively rare. In contrast to type-I core/shell quantum dots (QDs) possessing band offsets in that the conduction band of the shell is higher in energy than that of the core, while the relative energy level is opposite in the valence band, type-II QDs' valence and conduction bands in the core have both lower (or higher) than those in the shell materials⁹⁵ (see Figure 1.33). Thus, upon excitation, the carrier of type I is predominantly confined to the core, while the other is located in the shell. This spatial separation of charge carriers (electron and hole) leads to several characteristic differences from the type-I QDs. On the one hand, type-II structures allow reaching an interband emission with an energy gap that would be otherwise unavailable with type-I structures. On the other hand, the charge separation in type-II QDs should make these materials more suitable in, for example, photovoltaic applications, in which QDs may replace dye chromophores so that one of the photocarriers is injected from the QDs into a matrix before the occurrence of electron/hole recombination. Furthermore, because of the fluorescence emission of

type-II QDs can be tuned into near-infrared (NIR) region, they are widely used in bio-imaging applications. For example, Bawendi et al. in 2004 developed the use of NIR or infrared photons as a promising approach for biomedical imaging in

living tissue.^{96,97} They demonstrated that these type-II QDs allow a major cancer surgery, sentinel lymph nodemapping, to be performed in large animals under complete image guidance.

Most type-II nanocomposites reported have been grown by molecular beam epitaxy,^{98,99} which unfortunately limits its preparation in either one-dimensional or two-dimensional structures. Recently, based on a colloidal template (ie; TOPO), a seminal work on the chemical syntheses of type-II CdSe@ZnTe (core/shell) and CdTe@CdSe (core/shell) QDs using Cd(CH₃)₂ as a Cd precursor has been reported.⁹⁵ The soft-template approach provides both feasibility and versatility toward further chemical modification. In this thesis, we will discuss in **chapter 3**, the synthesis of CdSe@ZnTe (core/shell) type-II QDs via a greener precursor CdO is reported. Also, we will discuss their corresponding excited-state relaxation dynamics. The results reveal that the rate of photoinduced hole injection decreases as the size of the core increases, but independent of the thickness of the shell in the CdSe@ZnTe QDs. Note that in the case of CdSe@ZnTe QDs, both the valence and the conduction bands in the core are lower than those in the shell (see Figure 1.33).

A. Typical Type-I Quantum Dots (ex. CdSe/ZnS):



B. Type-II Quantum Dots (ex. CdSe/ZnTe, CdTe/CdSe):

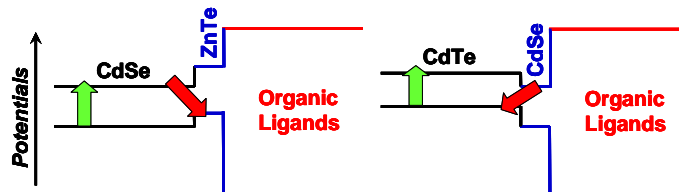
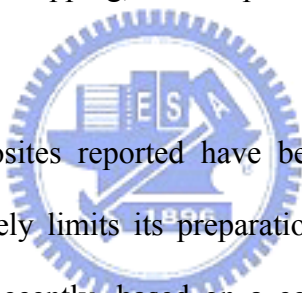
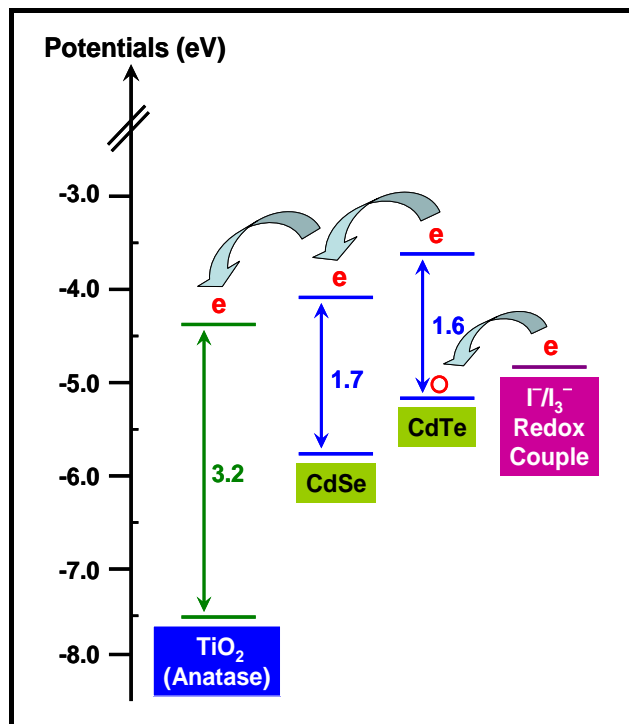


Figure 1.33 Illustrations of the energy band gap difference between (A) type-I and (B) type-II QDs.



Excited electrons in CdSe cannot circumvent the highly endergonic ZnTe conduction band. Thus, after electron hole migration the interband emission originates mainly from the CdSe (core) \rightarrow ZnTe (shell) transition, limiting its application toward photovoltaic device.



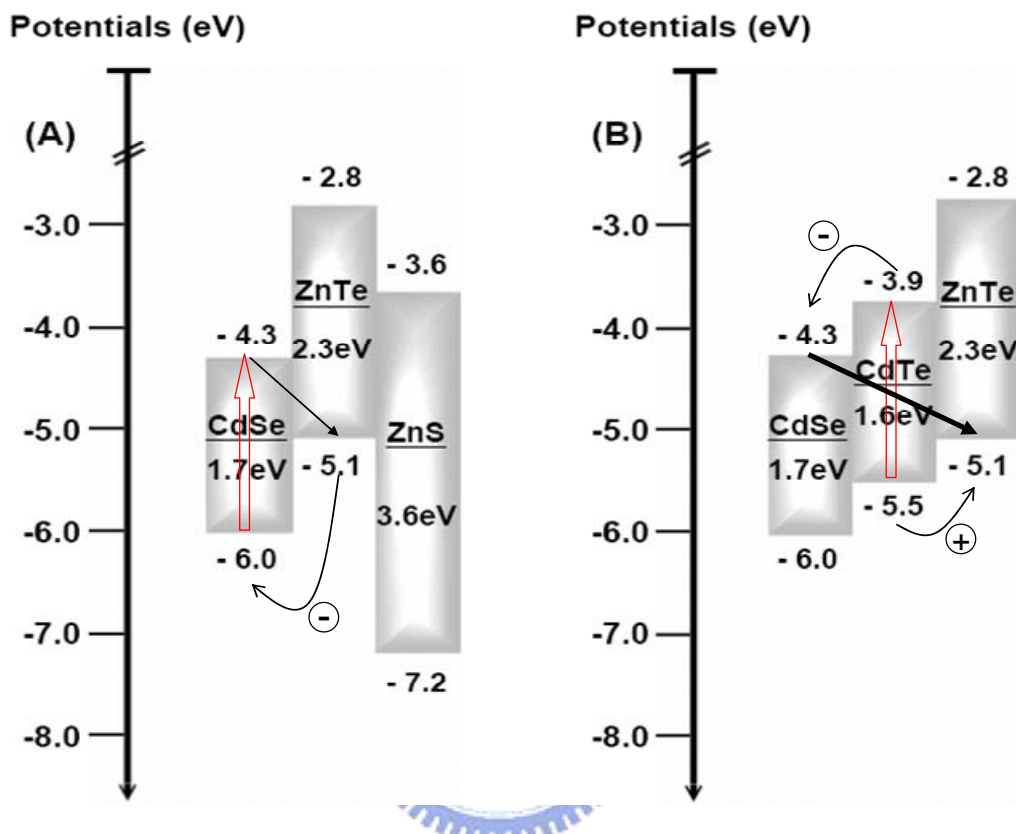
Scheme 1.1 Plot illustrating the CdTe, CdSe and TiO₂ band offsets alignment in energy. (e and o denote electron and hole, respectively)

Alternatively, in Chapter 3, we also report the other type-II QDs, CdTe@CdSe. Since both of its valence and conduction bands in the core are higher than those in the shell materials. Upon excitation, electron injection is likely to be from the conduction band of the shell (i.e. CdSe), providing a driving force to an electron acceptor. When properly constructed using TiO₂, commonly used in the dye sensitized solar energy cell (see Scheme 1.1), as the acceptor, an useful structure can be anticipated.

1.3.3. Type-II Core/Shell/Shell Quantum Dots

One disadvantage of using type-II QDs, such as CdSe@ZnTe, in applications, lies in its much weaker quantum efficiency in general. Since the interband emission originates from the spatially separated CdSe \rightarrow ZnTe transition, its associated radiative lifetime is expected to be long. Thus, any radiationless process, such as the floating of hole-carriers to the surface of the QDs, will drastically quench the

emission intensity. In order to enhance the quantum efficiency toward the NIR application, we will report in Chapter 4, the encapsulation of a third layer to achieve the CdSe@ZnTe@ZnS and CdSe@CdTe@ZnTe (core/shell/shell) structures.

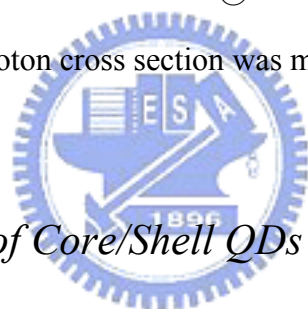


Scheme 1.2 Plot illustrating the CdSe, CdTe, ZnTe and ZnS band offsets alignment in energy. (Data are taken from ref. 100). Note that the changes of band gap and hence the relative energies in the interfacial regions are neglected in this diagram.

As shown in Scheme 1.2A, the conduction band in ZnTe is well above that in CdSe, while the valence band of ZnS is below that of ZnTe. Upon excitation, electron and hole are strictly confined in CdSe and ZnTe, respectively, encapsulated by ZnS. Thus, floating of the hole-carrier to the surface of ZnS can be significantly reduced, resulting in the enhancement of CdSe \rightarrow ZnTe interband emission intensity. In Scheme 1.2B, both valence and conduction bands in ZnTe are well above that in CdTe, forming a cascade type of band edges in a sequence of CdSe < CdTe < ZnTe. Upon excitation, electron and hole are eventually confined in CdSe and ZnTe, respectively. Thus, the lowest lying electron/hole combination, thermodynamically,

should originate from CdSe (electron) and ZnTe (hole). The rate of recombination is expected to be rather slow because charge separation is enhanced via an intermediate CdTe layer. Thus, in addition to its synthetic challenge and future chemistry perspectives, the associated photophysical properties of CdSe@CdTe@ZnTe (core/shell/shell) type II QDs are also of great importance. Detailed results will be discussed at Chapter 2.

Structural characterization of the synthesized Core@Shell@Shell QDs has been made via TEM, EDX, XPS and XRD. Photophysical properties were investigated via the absorption, interband emission and its associated quantum efficiency as well as relaxation dynamics. In view of applications in biomedical imaging, dihydrolipoic acid (DHLLA) encapsulated water soluble CdSe@ZnTe@ZnS QDs were also prepared and the corresponding two-photon cross section was measured.



1.4. The Applications of Core/Shell QDs Efforted in This Thesis

1.4.1. The Metal Ion Probes

Sensing toxic metal ions is essential in monitoring of the environment, the control of chemical processes, and medical applications. Of particular importance is the selective detection of the mercury ion (II), which is biologically highly toxic and is known to cause a variety of phenomena in humans, such as damage to the central nervous system and resulting neuropsychiatry disorders. Currently existing sensors for the detection of Hg^{2+} , such as thin-films device of gold,¹⁰¹ organic probes,^{102,103} polymeric material¹⁰⁴ and bio-composites,¹⁰⁵ are subject to certain inferiorities. These include high operation temperatures and complexity,¹⁰¹ latively low sensitivity, non-aqueous environments,^{102,106} and slow response due to the long-time equilibrium.¹⁰⁵ Ever since Pederson et al. discovered numerous metal ions could be

detected by cyclic polyethers (crown ethers) in 1967.¹⁰⁷ Numerous strategies of metal ion-sensors have been designed. Among these, organic fluorophores linked with ion recognition sites turn out to be the most popular metal ion probes. For example, our co-workers, P. T. Chou et al., developed a highly sensitive Ca^{2+} and Na^+ probe by anchoring organic fluorophore with a aza-crown that is suitable for the ion sizes, the design has achieved an excellent result (see Figure 1.34).¹⁰⁸ However, most of organic dyes acting as fluorophore tend to have narrow excitation spectra, and often exhibit broad emission bands with red tailing, which, due to spectral overlap, makes simultaneous quantitative evaluation of relative amounts of different probes present in the same sample difficult. To overcome such a barrier, Kim and co-workers have successfully prepared gold nanoparticles with the capability of sensing heavy metal ions.⁸¹ In their work, a simple colorimetric technique for the detection of small concentrations of aqueous heavy metal ions, including toxic metals such as lead, cadmium, and mercury was described. As depicted in Figure 1.35, they used 13.6 ± 0.4 nm diameter gold nanoparticles capped with 11-mercaptoundecanoic acid (MUA) as a probing system. Aqueous suspensions of the functionalized gold nanoparticles displayed intense plasmon absorptions that rendered the suspensions red. Aggregation of the particles (e.g. by addition of a metal ion salt solution) yielded both a shift in plasmon band energy and a substantial increase in long-wavelength Rayleigh scattering, resulting in a red-to-blue color shift (Figure 1.35).

Although this case successfully utilized gold nanoparticles as the metal ion probe, highly luminescent semiconductor QDs with broad excitation spectra and narrow, symmetric and tunable emission spectra could be superior to colorimetric metal ion sensor using gold nanoparticles. In 1996, Sooklal et al. demonstrated that manganese ion could be probed by ZnS QDs.¹⁰⁹ Similar works were performed by many groups employing quenching the fluorescence of semiconductor nanoparticles, $\text{CdS}^{110-112}$ and

CdTe.¹¹³ More recently, the group of Pang published two papers about the use of CdSe QDs and CdSe@ZnS QDs modified with bovine serum albumin (BSA)^{114,115} for Ag⁺ and Cu²⁺ detections, respectively. In Chapter 2,

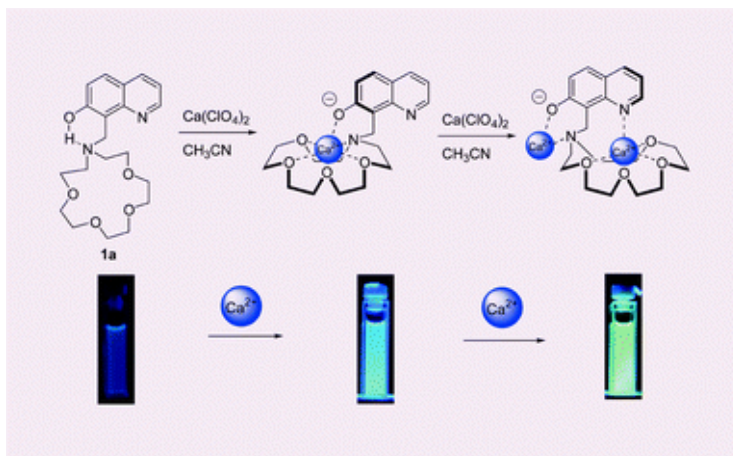


Figure 1.34 Metal ion probe by the organic fluorophore anchored with aza-crown.¹⁰⁸

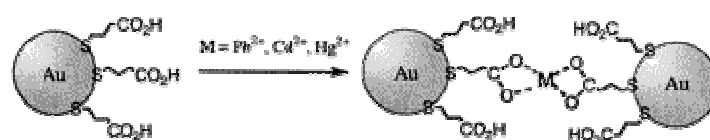


Figure 1.35 Heavy-metal ion recognition and binding of the functionalized gold nanoparticle.⁸¹

the design and the properties of the high sensitivity metal ion probes with type I core/shell QDs will be discussed.



1.4.2. Intermolecular Energy Transfer System

Furthermore, in order to extend the applications of type-I QDs, continuing the idea of metal ions probe by aza-crown,¹⁰⁸ (see Figure 1.34) we developed an energy transfer system with crown-dithio QDs. Herein, the Intermolecular Energy Transfer are briefly introduced as follows.

A. Aromatic Hydrocarbons

Among the hydrocarbons anthracene is probably one of the most thoroughly studied molecules. If anthracene solutions are irradiated in the absence of oxygen, the product is

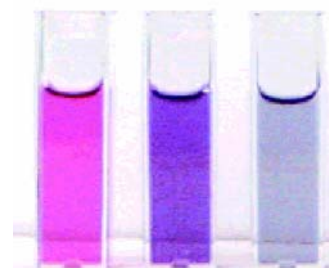


Figure 1.36 Colorimetric responses for metal ion recognition.¹⁰⁹

dianthracene. If oxygen is present, however, the product is the bridged peroxide. Furthermore, the photophysical properties of the novel hexapyropheophorbide a – fullerene hexaadduct (FHP6) compound (Figure 1.37) were studied by Röder et al. using both steady-state and time-resolved spectroscopic methods¹¹⁶. It was found that neighboring pyropheophorbide a (pyroPheo) molecules covalently linked to one fullerene moiety due to the length and high flexibility of carbon chains could stack with each other.

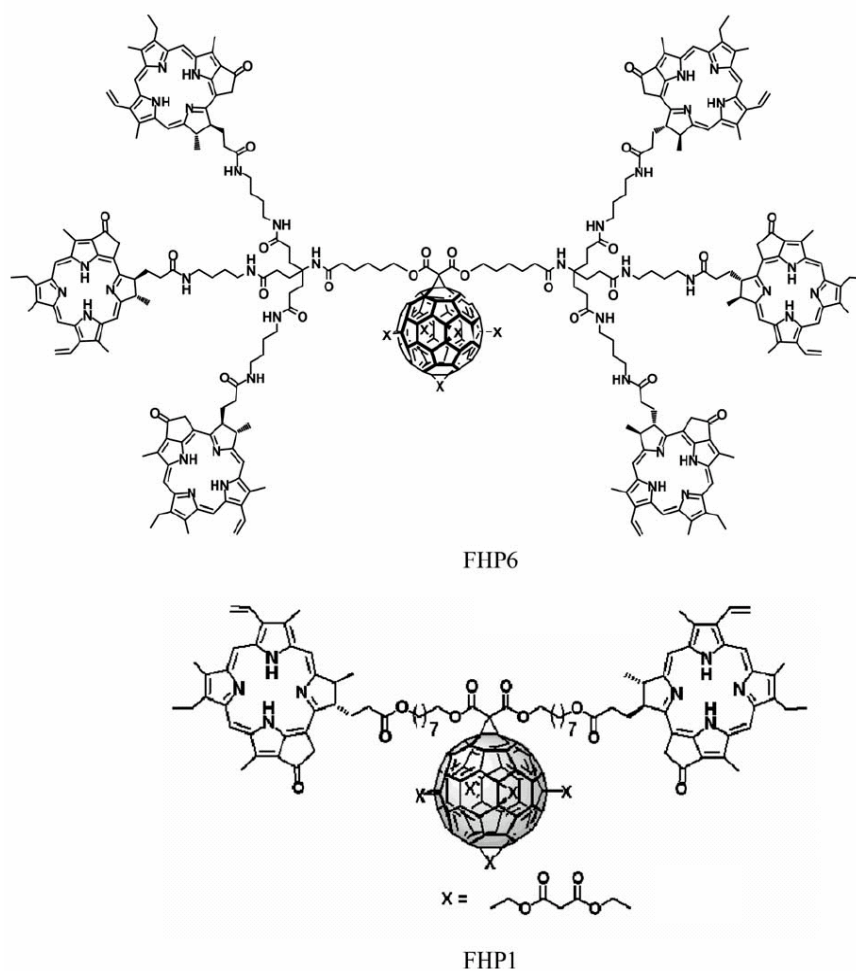


Figure 1.37 Structural formula of FHP6 and the reference compound FHP1.¹¹⁶

B. Carbonyls

Another important type of molecule participating in photochemistry is that containing the carbonyl group. Regioregular silylene-spaced copolymers

composed of an energy gradient with three different chromophores recently have been achieved by Yen-Ju Cheng and Tien-Yau Luh.¹¹⁷ Upon excitation of the donor chromophore (D1), only emission from the acceptor (A) was observed. Efficient and sequential energy transfer across three different chromophores along the polymeric backbone may proceed smoothly in these silylene-spaced copolymers. (Figure 1.38)

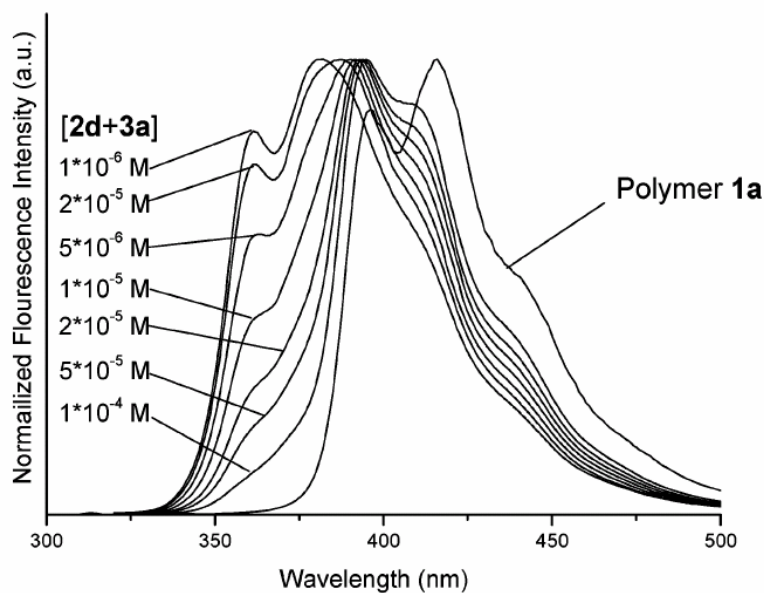


Figure 1.38 Concentration-dependent fluorescence spectra of an equal molar mixture of two compounds in CHCl_3 .¹¹⁷

C. Protein–protein interactions

A twofold increase in quenching constant was noted for KI quenching of AEDANS fluorescence emission in the presence of apoE CT domain, indicative of alterations in Ab conformation upon interaction with apoE CT domain. (See Figure 1.39) Narayanaswami, V. and his group¹¹⁸ propose intermolecular FRET (Fluorescence Resonance Energy Transfer) analysis as a discriminating approach to examine apoE/Ab interaction, a potentially critical factor in early events involved in amyloid formation.

The development of molecule-based ion sensors has been a pivotal issue currently receiving considerable attention. A prototypical detection scheme lies in two requirements, namely a sensing moiety with satisfactory ionic selectivity and the sensitivity, i.e. the measurable changes in response to the recognition. Among numerous methodologies, the exploitation of ionophores incorporated with optical transduction as a reporter seems to be a very promising one.¹¹⁹ In this approach, ionophores are usually coupled with a molecular chromophore, of which the associated spectral properties in either absorption or emission are sensitive to the environmental stimuli. Up to this stage, a large portion of chromophores being developed are hydrophobic, which consequently limits their applications in aqueous media. Recently, metal nanoparticles have been emerged as an important colorimetric reporter due to their extremely high extinction coefficient (i.e. absorptivity) that is also very sensitive to the transition from mono-dispersion to the aggregation, resulting in a distinct color change.^{52,81,120-124} For the case of gold nanoparticle, this phenomenon of which is well known as the surface plasmon absorption, the color change upon aggregation is due to the coupling of the surface plasmon resonance as a result of the proximity between two Au nanoparticles.^{125,126} Recently, based on a

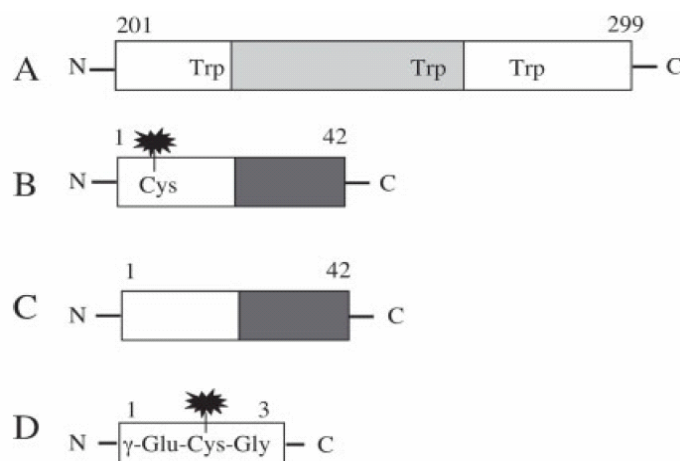


Figure 1.39 Fluorescence Resonance Energy Transfer Analysis of Apolipoprotein E C-Terminal.¹¹⁸

sandwich complex of 2:1 between 15-crown-5 and K^+ [12–19], Chen and coworkers¹²⁷ reported on capping the Au nanoparticles with the 15-crown-5 functionality and the resulting 15-crown-5 functionalized Au nanoparticles were successfully exploited as a novel prototype to probe K^+ , in which the transduction is signified by subtle changes of the surface plasma resonance, i.e. a colorimetry type of sensing mechanism. On this basis, other crown ether-modified metal nanoparticles, especially those of II-VI and III-V semiconductor composites, may serve as an alternative, taking advantages of their superior fluorescence properties such as high quantum efficiency and narrow bandwidth (good contrast luminescence color), etc. In Chapter 2, we report the design and synthesis of 15-crown-5 functionalized, water soluble CdSe/ZnS quantum dots (QDs) as well as their exploitation as a sensing unit toward K^+ in aqueous solution. The sensing mechanism utilizing either aggregation property in single size QDs as well as the Förster type of energy transfer in dual color QDs system renders a great versatility and flexibility in view of future applications.

1.5. References

1. Klabunde, K. J. *Free Atoms, Clusters, and Nanoscale Particles*, Academic Press, San Diego, 1994, pp.2, 36.
2. Klabunde, K. J.; Mohs, C. *Chemistry of Advanced Materials: An Overview*, Wiley-VCH, New York, 1998, p.271.
3. Ekimov, A. I.; Onuschenko, A. A. *Sov. Phys. Semicond.* **1982**, *16*, 775.
4. Rossetti, R.; Nakahara, S.; Brus, L. E. *J. Chem. Phys.* **1983**, *79*, 1086.
5. Alivisatos, A. P. *Science* **1996**, *271*, 933.

6. Alivisatos, A. P. *J. Phys. Chem.* **1996**, *100*, 13226.
7. (a) Henglein, A. *Chem. Rev.* **1989**, *89*, 1861. (b) Wang, Z. L.; Ahmad, T. S.; El-Sayed, M. A., *Surf. Sci.*, **1997**, *380*, 302.
8. Steigerwald, M. L.; Brus, L. E. *Acc. Chem. Res.* **1990**, *23*, 183.
9. Bawendi, M. G.; Steigerwald, M. L.; Brus, L. E. *Annu. Rev. Phys. Chem.* **1990**, *41*, 477.
10. Weller, H. *Angew. Chem., Int. Ed. Engl.* **1993**, *32*, 41.
11. Weller, H. *Adv. Mater.* **1993**, *5*, 88.
12. Hagfeldt, A.; Grätzel, M. *Chem. Rev.* **1995**, *95*, 49.
13. Fendler, J. H.; Meldrum, F. C. *Adv. Mater.* **1995**, *7*, 607.
14. Stroschio, J. A.; Eigler, D. M. *Science* **1991**, *254*, 1319.
15. Lieber, C. M.; Liu, J.; Sheehan, P. *Angew. Chem., Int. Ed. Engl.* **1996**, *35*, 687.
16. Trindade, T.; O'Brien, P.; Pickett, N. L. *Chem. Mater.* **2001**, *13*, 3843.
17. Haug, H.; Koch, S. W. *Quantum theory of the optical and electronic properties of semiconductors*; World Scientific Publishing Co. Pte. Ltd.: London, 1990, p. 333.
18. Éfros, Al. L.; Éfros, A. L. *Sov. Phys. Semicond.* **1982**, *16*, 772.
19. Brus, L. E. *J. Chem. Phys.* **1983**, *79*, 5566.
20. Brus, L. E. *J. Chem. Phys.* **1984**, *80*, 4403.
21. Brus, L. *J. Phys. Chem.* **1986**, *90*, 2555.
22. Colvin, V. L.; Schlamp, M. C.; Alivisatos, A. P. *Nature* **1994**, *420*, 800.
23. Schlamp, M. C.; Peng, X.; Alivisatos, A. P. *J. Appl. Phys.* **1997**, *82*, 5837.
24. Mattoussi, H.; Radzilowski, L. H.; Dabbousib, B. O.; Thomas, E. L.; Bawendi, M. G.; Rubner, M. F. *J. Appl. Phys.* **1998**, *83*, 7659.
25. Mattoussi, H.; Radzilowski, L. H.; Dabbousib, B. O.; Fogg, D. E.; Schrock, R. R.; Thomas, E. L.; Rubner, M. F.; Bawendi, M. G. *J. Appl. Phys.* **1999**, *86*, 4390.
26. Coe-Sullivan, S.; Woo, W.-K.; Steckel, J. S.; Bawendi, M. G.; Bulović, V. *Org. Electro.* **2003**, *4*, 123.

27. Seth Coe; Wing-Keung Woo; Mounji Bawendi; Vladimir Bulovic *Nature* **2002**, 420, 800.
28. Huynh, W. U.; Peng, X.; Alivisatos, A. P. *Adv. Mater.* **1999**, 11, 923.
29. Ginger, D. S.; Greenham, N. C. *Phys. Rev. B* **1999**, 59, 10622.
30. Huynh, W. U.; Dittmer, J. J.; Alivisatos, A. P. *Science* **2002**, 295, 2425.
31. Sun, B.; Marx, E.; Greenham, N. C. *Nano Lett.* **2003**, 3, 961.
32. Kumar, S.; Nann, T. *J. Mater. Res.* **2004**, 19, 1990.
33. Klimov, V. I.; Mikhailovsky, A. A.; Xu, Su.; Malko, A.; Hollingsworth, J. A.; Leatherdale, C. A.; Eisler, H.-J.; Bawendi, M. G. *Science* **2000**, 290, 314.
34. Klimov, V. I.; Mikhailovsky, A. A.; McBranch, D. W.; Leatherdale, C. A.; Bawendi, M. G. *Science* **2000**, 287, 1011.
35. Klimov, V. I.; Bawendi, M. G. *MRS Bulletin* **2001**, 26, 998.
36. Klimov, V. I. *Los Alamos Science* **2003**, 28, 214.
37. Xia, J. B.; *Phys. Rev. B* **1989**, 40, 8500.
38. Brus, L. E. *Appl. Phys. A* **1991**, 53, 465.
39. Wang, Y.; Herron, N.; *J. Phys. Chem.* **1991**, 95, 525.
40. Heath, J. R. *Science* **1992**, 258, 1131.
41. Wang, L. W.; Zunger, A. *Phys. Rev. B* **1996**, 53, 9579.
42. Leung, K.; Pokrant, S.; Whaley, K. B. *Phys. Rev. B* **1998**, 57, 12291.
43. Gaponenko, S. V. *Optical properties of semiconductor quantum dots*; Springer-Verlag: Berlin, 1996.
44. Nirmal, M.; Brus, L. E. *Acc. Chem. Res.* **1999**, 32, 407.
45. Elfros, Al. L. Rosen, M. *Annu. Rev. Mater. Sci.* **2000**, 30, 475.10.
46. Pankove, J. I. *Optical processes in semiconductors*; Dover Publications Inc.: New York, 1970.
47. Chestnoy, N.; Harris, T. D.; Hull, R.; Brus, L. E. *J. Phys. Chem.* **1986**, 90, 3393.
48. Nirmal, M.; Dabbousi, B. O.; Bawendi, M. G.; Macklin, J. J.; Trautman, J. K.; Harris, T. D.; Brus, L. E. *Nature* **1996**, 383, 802.
49. Bruchez Jr., M.; Moronne, M.; Gin, P.; Weiss, S.; Alivisatos, A. P. *Science* **1998**, 281, 2013.

50. Gerion, D.; Pinaud, F.; Williams, S. C.; Parak, W. J.; Zanchet, D.; Weiss, S.; Alivisatos, A. P. *J. Phys. Chem. B* **2001**, *105*, 8861.
51. Chan, W. C. W.; Nie, S. *Science* **1998**, *281*, 2016.
52. Mirkin, C. A.; Letsinger, R. L.; Mucic, R. C.; Storhoff, J. J. *Nature* **1996**, *382*, 607.
53. Storhoff, J. J.; Mucic, R. C.; Mirkin, C. A. *J. Clust. Sci.* **1997**, *8*, 179.
54. Storhoff, J. J.; Elghanian, R.; Mucic, R. C.; Mirkin, C. A.; Letsinger, R. L. *J. Am. Chem. Soc.* **1998**, *120*, 1959.
55. Mucic, R. C.; Storhoff, J. J.; Mirkin, C. A.; Letsinger, R. L. *J. Am. Chem. Soc.* **1998**, *120*, 12674.
56. Storhoff, J. J.; Mirkin, C. A. *Chem. Rev.* **1999**, *99*, 1849.
57. Mitchell, G. P.; Mirkin, C. A.; Letsinger, R. L. *J. Am. Chem. Soc.* **1999**, *121*, 8122.
58. Willard, D. M.; Carillo, L. L.; Jung, J.; Orden, A. V. *Nano Lett.* **2001**, *1*, 469.
59. Parak, W. J.; Boudreau, R.; Le Gros, M.; Gerion, D.; Zanchet, D.; Micheel, C. M.; Williams, S. C.; Alivisatos, A. P.; Larabell, C. *Adv. Mater.* **2002**, *14*, 882.
60. Chan, W. C. W.; Maxwell, D. J.; Gao, X.; Bailey, R. E.; Han, M.; Nie, S. *Curr. Opin. Biotechnol.* **2002**, *13*, 40.
61. Åkerman, M. E.; Chan, W. C. W.; Laakkonen, P.; Bhatia, S. N.; Ruoslahti, E. *Proc. Natl. Acad. Sci. USA* **2002**, *99*, 12617.
62. Dubertret, B.; Skourides, P.; Norris, D. J.; Noireaux, V.; Brivanlou, A. H.; Libchaber, A. *Science* **2002**, *298*, 1759.
63. Larson, D. R.; Zipfel, W. R.; Williams, R. M.; Clark, S. W.; Bruchez, M. P.; Wise, F. W.; Webb, W. W. *Science* **2003**, *300*, 1434.
64. Wu, X.; Liu, H.; Liu, J.; Haley, K. N.; Treadway, J. A.; Larson, J. P.; Ge, N.; Peale, F.; Bruchez, M. P. *Nat. Biotechnol.* **2003**, *21*, 41.

65. Jaiswal, J. K.; Mattoussi, H.; Mauro, J. M.; Simon, S. M. *Nat. Biotechnol.* **2003**, *21*, 47.
66. Han, M.; Gao, X.; Su, J. Z.; Nie, S. *Nat. Biotechnol.* **2001**, *19*, 631.
67. Mattoussi, H.; Mauro, J. M.; Goldman, E. R.; Anderson, G. P.; Sundar, V. C.; Mikulec, F. V.; Bawendi, M. G. *J. Am. Chem. Soc.* **2000**, *122*, 12142.
68. Winter, J. O.; Liu, T. Y.; Korgel, B. A.; Schmidt, C. E. *Adv. Mater.* **2001**, *13*, 1673.
69. Rosenthal, S. J.; Tomlinson, I.; Adkins, E. M.; Schroeter, S.; Adams, S.; Swafford, L.; McBride, J.; Wang, Y.; DeFelice, L. J.; Blakely, R. D. *J. Am. Chem. Soc.* **2002**, *124*, 4586.
70. Goldman, E. R.; Balighian, E. D.; Mattoussi, H.; Kuno, M. K.; Mauro, J. M.; Tran, P. T.; Anderson, G. P. *J. Am. Chem. Soc.* **2002**, *124*, 6378.
71. Chen, Y.; Ji, T.; Rosenzweig, Z. *Nano Lett.* **2003**, *3*, 581.
72. Derfus, A. M.; Chan, W. C. W.; Bhatia, S. N. *Nano Lett.* **2004**, *4*, 11.
73. Clapp, A. R.; Medintz, I. L.; Mauro, J. M.; Fisher, B. R.; Bawendi, M. G.; Mattoussi, H. *J. Am. Chem. Soc.* **2004**, *126*, 301.
74. Hong, R.; Fischer, N. O.; Verma, A.; Goodman, C. M.; Emrick, T.; Rotello, V. *M. J. Am. Chem. Soc.* **2004**, *126*, 739.
75. Pinaud, F.; King, D.; Moore, H. P.; Weiss, S. *J. Am. Chem. Soc.* **2004**, *126*, 6115.
76. Niemeyer, C. M. *Angew. Chem., Int. Ed. Engl.* **2001**, *40*, 4128.
77. Murphy, C. J. *Anal. Chem. A-Pages* **2002**, *74*, 520A.
78. Jovin, T. M. *Nat. Biotechnol.* **2003**, *21*, 32.
79. Riegler, J.; Nann, T. *Anal. Bioanal. Chem.* **2004**, *379*, 913.
80. Green, M. *Angew. Chem., Int. Ed. Engl.* **2004**, *43*, 4129.
81. Kim, Y.; Johnson, R. C.; Hupp, J. T. *Nano Lett.* **2001**, *1*, 165.

82. Aldana, J.; Wang, Y. A.; Peng, X. *J. Am. Chem. Soc.* **2001**, *123*, 8844.
83. Sundar, V. C.; Eisler, H.-J.; Bawendi, M. G. *Adv. Mater.* **2002**, *14*, 739.
84. Petruska, M. A.; Malko, A. V.; Voyles, P. M.; Klimov, V. I. *Adv. Mater.* **2003**, *15*, 610.
85. Petruska, M. A.; Bartko, A. P.; Klimov, V. I. *J. Am. Chem. Soc.* **2004**, *126*, 714.
86. Gao, X.; Gui, Y.; Levenson, R. M.; Chung, L. W. K.; Nie, S. *Nat. Biotechnol.* **2004**, *22*, 969.
87. Pellegrino, T.; Manna, L.; Kudera, S.; Liedl, T.; Koktysh, D.; Rogach, A. L.; Keller, S.; Rädler, J.; Natile, G.; Parak, W. J. *Nano Lett.* **2004**, *4*, 703.
88. Jaffar, S.; Nam, K. T.; Khademhosseini, A.; Xing, J.; Langer, R. S.; Belcher, A. M. *Nano Lett.* **2004**, *4*, 1421.
89. Hong, X.; Li, J.; Wang, M.; Xu, J.; Guo, W.; Li, J.; Bai, Y.; Li, T. *Chem. Mater.* **2004**, *16*, 4022.
90. Peng, X.; Schlamp, M. C.; Kadavanich, A. V.; Alivisatos, A. P. *J. Am. Chem. Soc.* **1997**, *119*, 7019.
91. Dabbousi, B. O.; Rodriguez-Viejo, J.; Mikulec, F. V.; Heine, J. R.; Mattoussi, H.; Ober, R.; Jensen, K. F.; Bawendi, M. G. *J. Phys. Chem. B* **1997**, *101*, 9463.
92. Guo, W.; Li, J. J.; Wang, Y. A.; Peng, X. *J. Am. Chem. Soc.* **2003**, *125*, 3901.
93. Underwood, D. F.; Kippeny, T.; Rosenthal, S. J. *J. Phys. Chem. B* **2001**, *105*, 436.
94. Cao, Y. W.; Banin, U. *J. Am. Chem. Soc.* **2000**, *122*, 9692.
95. Kim, S.; Fisher, B.; Eisler, H. J.; Bawendi, M. G. *J. Am. Chem. Soc.* **2003**, *125*, 11466.
96. Lim, Y. T.; Kim, S.; Nakayama, A.; Stott, N. E.; Bawendi, M. G.; Frangioni, J. V. *Mol. Imaging* **2003**, *2*, 50.
97. Kim, S.; Lim, Y. T.; Soltesz, E. G.; De Grand, A. M.; Lee, J.; Nakayama, A.;

- Parker, J. A.; Mihaljevic, T.; Laurence, R. G.; Dor, D. M.; Cohn, L. H.; Bawendi, M. G.; Frangioni, J. V. *Nat. Biotechnol.* **2004**, *22*, 93.
98. Hatami, F.; Grundmann, M.; Ledentsov, N. N.; Heinrichsdorff, F.; Heitz, R.; Böhrer, J.; Bimberg, D.; Ruvimov, S. S.; Werner, P.; Ustinov, V. M.; Kop'ev, P. S.; Alferov, Z. I. *Phys. Rev. B* **1998**, *57*, 4635.
99. Youn, H. C.; Baral, S.; Fendler, J. H. *J. Phys. Chem.* **1998**, *92*, 6320.
100. S. J. Pearton, *Wide bandgap semiconductors*, William Andrew Publishing, NY, 2000, p.9.
101. Braininaa, K. Z.; Stozhko, N. Y.; Shlygina, Z. V. *J. Anal. Chem.* **2002**, *57*, 945.
102. Yoon, J.; Ohler, N. E.; Vance, D. H.; Aumiller, W. D.; Czarnic, A. W. *Tetrahedron Lett.* 1997, *38*, 3845.
103. Descalzo, A. B.; Martinez-Mañez, R.; Redeglia, R.; Rurack, K.; Sato, J. *J. Am. Chem. Soc.* 2003, *125*, 3418.
104. Wang, X.; Lee, C.; Soo-Hyoung, S.; Kris, J.; Kumar, J.; Samuelson, L. *Nano Lett.* **2002**, *2*, 1273.
105. Shi, G.; Jiang, G. *Anal. Sci.* **2002**, *18*, 1215.
106. Chae, M.-Y.; Czarnic, A. W. *J. Am. Chem. Soc.* **1992**, *114*, 9704.
107. Pederson, C. J. *J. Am. Chem. Soc.* **1967**, *89*, 7017.
108. Wu, K. C.; Ahmed, M. O.; Chen, C. Y.; Huang, G. W.; Hon, Y. S.; Chou, P. T. *Chem. Commun.* **2003**, 890.
109. Sooklal, K.; Cullum, B. S.; Angel, S. M.; Murphy, C. J. *J. Phys. Chem.* **1996**, *100*, 4551.
110. Diaz, D.; Robles, J.; Ni, T.; Castillo-Blum, S.; Nagesha, D.; Alvarez-Fregoso, O.; Kotov, N. *J. Phys. Chem. B* **1999**, *103*, 9859.
111. Moore, D. E.; Patel, K. *Langmuir* **2001**, *17*, 2541.
112. Chen, Y.; Rosenzweig, Z. *Anal. Chem.* **2002**, *74*, 5132.

113. Gao, M.; Kirstein, S.; Möhwald, H.; Rogach, A.; Kornowski, A.; Eychmüller, A.; Weller, H. *J. Phys. Chem. B* **1998**, *102*, 8360.
114. Liang, J. G.; Ai, X. P.; He, Z. K.; Pang, D. W. *Analyst* **2004**, *129*, 619.
115. Xie, H. Y.; Liang, J. G.; Zhang, Z. L.; Liu, Y.; He, Z. K.; Pang, D. W. *Spectrochimica Acta Part A* **2004**, *60*, 2527.
116. Ermilov, E.A.; Hackbarth, St.; Al-Omari, S.; Helmreich, M.; Jux, N.; Hirsch, A.; Röder, B., *Optics Communications*, **2005**, *250*, 95.
117. Cheng, Y.J.; Luh, T.Y., *Macromolecules*, **2005**, *38*, 4563.
118. Phu, M.J.; Hawbecker, S.K.; Narayanaswam, V.i, *J. Neuroscience Research*, **2005**, *80*, 877.
119. For the recent review, see Steed, J. W.; Atwood, J. L. *Supramolecular Chemistry*; John Wiley & Sons: New York, 2000.
120. Brust, M.; Bethell, D.; Schiffrin, D. J.; Kiely, C. J. *Adv. Mater.* **1995**, *7*, 795-797.
121. Grabar, K. C.; Freeman, R. G.; Hommer, M. B.; Natan, M. J. *Anal. Chem.* **1995**, *67*, 735-743.
122. Elghanian, R.; Storhoff, J. J.; Mucic, R. C.; Letsinger, R. L.; Mirkin, C. A. *Science* **1997**, *277*, 1078-1081.
123. Link, S.; El-Sayed, M. A. *J. Phys. Chem. B* **1999**, *103*, 8410-8426.
124. Demers, L. M.; Mirkin, C. A.; Mucic, R. C.; Reynolds, R. A., III; Letsinger, R. L.; Elghanian, R.; Viswanadham, G. *Anal. Chem.* **2000**, *72*, 5535-5541.
125. Kreibig, U.; Vollmer, M. *Optical Properties of Metal Clusters*; Springer: Berlin, 1995.
126. Storhoff, J. J.; Lazarides, A. A.; Mucic, R. C.; Mirkin, C. A.; Letsinger, R. L.; Schatz, G. C. *J. Am. Chem. Soc.* **2000**, *122*, 4640-4650.
127. Lin, S. Y.; Liu, S. W.; Lin, C. M.; Chen, C. H. *Anal. Chem.* **2002**, *74*, 330-335.